Available online at www.sciencedirect.com

SciVerse ScienceDirect

Geochimica et Cosmochimica Acta 99 (2012) 287–304

Geochimica et Cosmochimica Acta

www.elsevier.com/locate/gca

Hf–W chronometry of core formation in planetesimals inferred from weakly irradiated iron meteorites

Thomas S. Kruijer [a,b,*], Peter Sprung [a,b], Thorsten Kleine [b], Ingo Leya [c], Christoph Burkhardt [a], Rainer Wieler [a]

[a] ETH Zürich, Institute of Geochemistry and Petrology, Clausiusstrasse 25, 8092 Zürich, Switzerland
[b] Institut für Planetologie, Westfälische Wilhelms-Universität Münster, Wilhelm-Klemm-Strasse 10, 48149 Münster, Germany
[c] Space Research and Planetary Sciences, University of Bern, Sidlerstrasse 5, 3012 Bern, Switzerland

Received 16 January 2012; accepted in revised form 5 September 2012; available online 25 September 2012

Abstract

The application of Hf–W chronometry to determine the timescales of core formation in the parent bodies of magmatic iron meteorites is severely hampered by ^{182}W burnout during cosmic ray exposure of the parent meteoroids. Currently, no direct method exists to correct for the effects of ^{182}W burnout, making the Hf–W ages for iron meteorites uncertain. Here we present noble gas and Hf–W isotope systematics of iron meteorite samples whose W isotopic compositions remained essentially unaffected by cosmic ray interactions. Most selected samples have concentrations of cosmogenic noble gases at or near the lowermost level observed in iron meteorites and, for iron meteorite standards, have very low noble gas and radionuclide based cosmic ray exposure ages (<60 Ma). In contrast to previous studies, no corrections of measured W isotope compositions are required for these iron meteorite samples. Their $\varepsilon^{182}W$ values (parts per 10^4 deviations from the terrestrial value) are higher than those measured for most other iron meteorites and range from −3.42 to −3.31, slightly elevated compared to the initial $^{182}W/^{184}W$ of Ca–Al-rich Inclusions (CAI; $\varepsilon^{182}W = -3.51 \pm 0.10$). The new W isotopic data indicate that core formation in the parent bodies of the IIAB, IIIAB, and IVA iron meteorites occurred ~1–1.5 Myr after CAI formation (with an uncertainty of ~1 Myr), consistent with earlier conclusions that the accretion and differentiation of iron meteorite parent bodies predated the accretion of most chondrite parent bodies. One ungrouped iron meteorite (Chinga) exhibits small nucleosynthetic W isotope anomalies, but after correction for these anomalies its $\varepsilon^{182}W$ value agrees with those of the other samples. Another ungrouped iron (Mbosi), however, has elevated $\varepsilon^{182}W$ relative to the other investigated irons, indicating metal–silicate separation ~2–3 Myr later than in the parent bodies of the three major iron meteorite groups studied here.

1. INTRODUCTION

Magmatic iron meteorites are interpreted as fragments from the metal cores of small planetary bodies (Scott, 1972; Scott and Wasson, 1975) that had formed early in solar system history (e.g., Chen and Wasserburg, 1990; Smoliar et al., 1996; Kleine et al., 2005a). Obtaining a precise chronology of iron meteorites, therefore, is of fundamental importance for constraining the early history of the solar system, and the accretion and differentiation history of some of the earliest planetesimals. The short-lived ^{182}Hf–^{182}W system has proven uniquely useful for determining the timescales of core formation in planetary bodies, because both Hf and W are refractory and exhibit very different geochemical behaviour during metal–silicate separation (e.g., Lee and Halliday, 1995; Harper and Jacobsen, 1996; Kleine et al., 2009). The first comprehensive Hf–W study on iron meteorites was performed by Horan et al. (1998), showing that the different iron meteorite parent bodies underwent core formation within ~5 Myr of each

* Corresponding author at: ETH Zürich, Institute of Geochemistry and Petrology, Clausiusstrasse 25, 8092 Zürich, Switzerland. Tel.: +41 44 63 26423, +49 251 83 39708.
E-mail address: thomas.kruijer@erdw.ethz.ch (T.S. Kruijer).

0016-7037/$ - see front matter © 2012 Elsevier Ltd. All rights reserved.
http://dx.doi.org/10.1016/j.gca.2012.09.015

other. Later studies demonstrated that magmatic iron meteorites derive from planetesimals that segregated their cores very early (e.g., Kleine et al., 2005a; Scherstén et al., 2006; Markowski et al., 2006b; Qin et al., 2008b), at about the same time as Ca–Al-rich inclusions (CAI), the oldest yet dated objects that formed in the solar system (Gray et al., 1973; Amelin et al., 2010; Bouvier and Wadhwa, 2010). The chronological interpretation of the Hf–W data for iron meteorites is severely complicated, however, by ^{182}W burnout due to capture of secondary thermal and epithermal neutrons produced during cosmic ray exposure of the iron meteoroids (Masarik, 1997; Leya et al., 2000, 2003). The most obvious manifestation of these neutron capture reactions is the decrease of $^{182}W/^{184}W$ ratios of iron meteorites with increasing cosmic ray exposure age, leading to spuriously old Hf–W model ages. Neutron capture on W isotopes may be responsible for generating $^{182}W/^{184}W$ ratios lower than the initial W isotope composition of CAI (Burkhardt et al., 2008, 2012) and may also be the sole cause of ^{182}W variations observed within individual iron meteorite groups or even within a single iron meteorite. The reliable interpretation of W isotopic data for iron meteorites in terms of core formation timescales, therefore, requires the quantification of cosmic ray-induced shifts on W isotope compositions.

The interaction of iron meteoroids with cosmic rays did not only cause neutron capture reactions on W isotopes but also led to the production of cosmogenic noble gases. For this reason, a number of studies focused on cosmogenic noble gases and published cosmic ray exposure ages to correct measured W isotope compositions for cosmic ray-induced shifts (Kleine et al., 2005a; Scherstén et al., 2006; Markowski et al., 2006a; Qin et al., 2008b). For instance, Markowski et al. (2006a) used ^{3}He abundances in conjunction with independently determined exposure ages to correct measured W isotope compositions in Carbo (IID) and Grant (IIIAB). However, the corrected $^{182}W/^{184}W$ of these two iron meteorites still are lower than the initial W isotope composition of CAI (Burkhardt et al., 2008, 2012). At face value this would indicate core formation of the respective parent bodies to predate CAI formation. However, more likely this strongly suggests that the correction procedure employing ^{3}He did not fully account for cosmic ray-induced W isotope shifts. Qin et al. (2008b) estimated lower and upper bounds of $^{182}W/^{184}W$ ratios for several groups of magmatic iron meteorites and modelled a maximum expected cosmogenic W isotope effect for a given exposure age. For all iron meteorite groups the upper bounds on $^{182}W/^{184}W$ were found to be higher than the presently accepted initial $^{182}W/^{184}W$ of CAI (Burkhardt et al., 2012), solving the problem that some iron meteorites have measured $^{182}W/^{184}W$ below the CAI initial. However, the difference between the lower and upper bounds of $^{182}W/^{184}W$ ratios for individual iron meteorite groups remaining after this correction corresponds to apparent 2–5 Myr intervals of metal segregation (e.g., for IC, IIAB, IID, IIIF, IVA irons), reflecting the inherent uncertainty of current correction procedures employing noble gas systematics.

The major problem when using cosmogenic noble gases and/or exposure ages to correct cosmic ray-induced shifts in $^{182}W/^{184}W$ is that cosmogenic noble gas production rates reach their maximum at a shallower depth than that corresponding to the maximum fluence of thermal and epithermal secondary neutrons. Cosmogenic noble gases are thus not a perfect proxy for the fluence of slow neutrons. Obtaining a precise Hf–W chronometry of iron meteorites thus requires the development of a direct neutron dosimeter for iron meteorites, or the identification of specimens that remained largely unaffected by (epi)thermal neutrons. While recent studies have shown that Os (Walker and Touboul, 2012; Wittig et al., 2012) and Pt isotopes (Kruijer et al., 2012) may be suitable neutron dosimeters for iron meteorites, we here will focus on identifying iron meteorite specimens with minor to absent (epi)thermal neutron fluences. Such samples do not require any correction on measured W isotope ratios and thus present key samples for establishing a precise Hf–W chronology of iron meteorites.

Although cosmogenic noble gases do not allow a precise and accurate correction for cosmic ray-induced neutron capture effects on W isotopes, they do provide very useful constraints on the cosmic ray exposure history of meteorites. In some cases noble gas data allow recognising meteorites with a very low exposure age (for iron meteorite standards). Such meteorites will have experienced a very low (epi)thermal neutron fluence irrespective of the sample position within the meteoroid. Therefore, in this contribution we use concentrations of cosmogenic He, Ne, and Ar in samples of magmatic iron meteorites from different groups as major selection criteria to identify specimens with W isotopic compositions largely unaffected by cosmic ray effects. New precise W isotope measurements on these samples that define $^{182}W/^{184}W$ values devoid of cosmic ray effects are then used to obtain improved constraints on the timing and duration of core formation in iron meteorite parent bodies.

2. THEORY AND APPROACH

Interactions of highly energetic (primary) cosmic ray particles (~0.1–~10 GeV) with target atoms in meteoroids generate a cascade of nuclear reactions. Among other products this yields secondary high-energy protons and neutrons in the energy range of a few to a few hundred MeV. The primary and secondary high-energy particles produce cosmogenic nuclides, mostly by spallation-type reactions. Important for this study is the production of cosmogenic noble gas isotopes, whose concentrations are a measure for the fluence of medium- to high-energy particles in the sample. At the same time, the secondary cosmic ray particles are slowed down, either due to electronic stopping in the case of secondary protons or by elastic scattering in the case of secondary neutrons. The latter are thus moderated to epithermal (~0.025 eV to a few keV) and eventually to thermal (~0.025 eV at 293 K) energies with increasing distance from the meteoroid surface (Lingenfelter et al., 1972; Leya et al., 2000). Tungsten isotopes are predominantly affected by neutron capture reactions at epithermal energies (Masarik, 1997; Leya et al., 2000, 2003), and possess different abilities to capture epithermal neutrons,

expressed as distinct resonance integrals (e.g., at $T = 300$ K: ^{182}W ~600 barns, ^{183}W ~355 barns, ^{184}W ~16 barns, ^{186}W ~520 barns; ENDFB-VI.8 300K library, 0.5 eV to 1×10^5 eV). The maximum fluence of thermal and epithermal neutrons occurs at larger depth than the maximum production of noble gases. Therefore, cosmogenic noble gases are not a direct measure for neutron capture-induced shifts on W isotopes.

As the majority of iron meteorites have been exposed to cosmic rays for longer than 100 Myr (and up to 2 Gyr) (e.g., Voshage, 1978, 1984; Wieler, 2002; Eugster, 2003), the expected cosmic ray effects on W isotopes will be more pronounced than in stony meteorites (e.g., Leya et al., 2000, 2003). Moreover, the iron-dominated matrix promotes neutron energy spectra that are biased towards epithermal energies (Kollár et al., 2006; Sprung et al., 2010) at which W isotopes are most susceptible to neutron capture. In stony meteorites and lunar rocks W isotope ratios are predominantly affected by the neutron capture reaction ^{181}Ta(n,γ)^{182}Ta(β$^-$)^{182}W, resulting in elevated ^{182}W/^{184}W ratios (e.g., Leya et al., 2000, 2003). This reaction is responsible for generating large ^{182}W excesses in lunar rocks (Lee et al., 2002; Kleine et al., 2005b). Since Ta is not present in Fe–Ni metal, neutron capture reactions that have W isotopes as their target (e.g., ^{182}W(n,γ)^{183}W, ^{183}W(n,γ)^{184}W, ^{184}W(n,γ)^{185}W(β$^-$)^{185}Re, ^{186}W(n,γ)^{187}W(β$^-$)^{187}Re) dominate in iron meteorites (Masarik, 1997; Leya et al., 2000). Neutron capture reactions in iron meteorites induce a negative shift in ^{182}W/^{184}W and a positive shift in ^{183}W/^{184}W. The correction for instrumental mass discrimination (using either ^{186}W/^{183}W or ^{186}W/^{184}W), however, tends to largely cancel out the effect on ^{183}W/^{184}W ratios, while magnifying the effect on ^{182}W/^{184}W. Internal corrections for cosmic ray-induced neutron capture effects (i.e., using W isotopes only) are thus not possible.

Given the difficulty in quantifying cosmic ray-induced neutron capture effects on W isotopes, the pre-exposure ^{182}W/^{184}W ratio of magmatic iron meteorites would ideally be determined on samples largely unaffected by such neutron capture reactions. Cosmogenic noble gases – although not suitable for correcting neutron capture effects on W isotopes – are useful to identify such samples. First, in some cases the combination of a noble gas and a radionuclide allows the determination of the production rate of the noble gas nuclide at the sample position and hence a reliable shielding-corrected exposure age of the meteorite. Two of the meteorites in this study (Braunau, IIAB, and Gibeon, IVA) were selected according to their exposure ages being below 60 Ma as determined by previous workers with this approach (e.g., Cobb, 1966; Chang and Wänke, 1969; Honda et al., 2009). As demonstrated in Section 5, such samples will have very small if any neutron capture effects on their W isotopic composition. A third meteorite studied here (Cape York, IIIAB) has a slightly higher exposure age of about 90 Ma (Mathew and Marti, 2009), but we will demonstrate that the W isotope compositions of the Cape York samples investigated here also remained essentially unaffected by cosmic ray effects. Overall, iron meteorites with shielding-corrected very low exposure ages are rare, however.

Second, noble gases in iron meteorites provide information about meteoroid size and sampling depth, as ratios like ^{4}He/^{21}Ne or ^{3}He/^{4}He depend on these parameters (e.g., Signer and Nier, 1960). In the present study, such parameters must be used with caution, however, because the very low noble gas concentrations (sometimes close to blank levels) often lead to large analytical uncertainties. Nevertheless, for most of the specimens studied here, the He, Ne, and Ar concentration and isotopic composition analyses permit semi-quantitative estimates on the pre-atmospheric size, sample location in the meteoroid and maximum possible cosmic ray exposure age.

3. ANALYTICAL METHODS

3.1. Sample selection

Magmatic iron meteorites whose reported cosmogenic noble gas concentrations are consistently at the lower end of the range observed in iron meteorites (Schultz and Franke, 2004) were selected for this work. The samples investigated here include iron meteorite specimens from four different magmatic groups (IIAB, IIIAB, IVA, IIG) and two ungrouped iron meteorites (Tables 1 and 3). Noble gas concentrations were re-measured for all of the meteorite specimens investigated in this study in material that had been in immediate contact to that used for W isotope analysis.

3.2. Noble gas measurements

Extraction and measurement of He, Ne and Ar concentrations and isotope compositions were performed at the University of Bern. Analytical procedures are outlined in Ammon et al. (2008, 2011). Iron meteorite samples (50–160 mg) were cut using a diamond saw, cleaned ultrasonically in ethanol (5 min), and wrapped in commercial Ni-foil. Extraction of He, Ne and Ar was performed by heating the samples at 1700–1800 °C in a Mo-crucible for 35 min. A boron-nitride liner placed inside the Mo crucible helped to avoid corrosion of the Mo crucible. Extracted gases were cleaned using various Ti-getters and activated charcoal. The Ar fraction was separated from He and Ne using activated charcoal (at −196 °C). Helium and Ne were measured in a 90° sector field mass spectrometer and Ar in a tandem mass spectrometer with two 90° magnetic sector fields. Both non-commercial mass spectrometers have Nier-type ion sources and are equipped with a Faraday collector and an electron multiplier working in analogue mode. Since the noble gas amounts of the studied samples are low, only electron multiplier measurements were used. Noble gas concentrations were determined by peak height comparison to calibrated standard gases that are isotopically similar to atmospheric composition (only ^{3}He is elevated relative to atmospheric composition). Calibration gases were measured before or after each sample analysis. All ^{20}Ne signals were corrected for interferences from $H_2{}^{18}O$. The sensitivity of the mass spectrometers used in this study varies non-linearly as a function of total gas pressure. The measured He and Ne amounts were corrected for this effect using

Table 1
Cosmogenic noble gas concentrations of iron meteorites samples investigated in this study.

Meteorite name	ID	^{3}He [±1SD] [10^{-8} cm^{3}STP/g]	^{4}He [±1SD] [10^{-8} cm^{3}STP/g]	$^{21}Ne_{cos}$ [±1SD] [10^{-8} cm^{3}STP/g]	$^{38}Ar_{cos}$ [±1SD] [10^{-8} cm^{3}STP/g]	^{4}He/$^{21}Ne_{cos}$ [±1SD] [10^{-8} cm^{3}STP/g]	^{3}He/^{4}He [±1SD] [10^{-8} cm^{3}STP/g]
IIAB irons							
Edmonton (Canada)	A02	0.290 ± 0.029	3.25 ± 0.39	0.011 ± 0.006	0.057 ± 0.006	na	0.09 ± 0.01
Braunau	M03	2.41 ± 0.15	24.8 ± 1.5	0.17 ± 0.03	0.645 ± 0.048	150 ± 29	0.10 ± 0.01
Sikhote Alin 'SA01'	B01	133 ± 9	561 ± 38	2.61 ± 0.20	14.5 ± 0.95	215 ± 22	0.24 ± 0.02
Sikhote Alin 'SA02'	G03a	12.7 ± 0.68	58.3 ± 3.1	0.22 ± 0.03	1.22 ± 0.079	265 ± 40	0.22 ± 0.02
Sikhote Alin 'SA02'	G03b	13.7 ± 0.76	63.6 ± 3.5	0.25 ± 0.04	1.12 ± 0.074	255 ± 45	0.22 ± 0.02
IIIAB irons							
Cape York 'CY01'	A01	0.574 ± 0.043	3.47 ± 0.31	0.006 ± 0.004	0.042 ± 0.004	na	0.17 ± 0.02
Cape York 'CY02'	G02a	0.229 ± 0.019	2.02 ± 0.17	0.005 ± 0.001	0.017 ± 0.011	410 ± 104	0.11 ± 0.01
Cape York 'CY02'	G02b	0.220 ± 0.021	1.57 ± 0.15	0.005 ± 0.001	0.025 ± 0.003	320 ± 91	0.14 ± 0.02
IVA irons							
Gibeon '102'	N02	<Detection	<Detection	<Detection	0.0003 ± 0.0003	na	na
Muonionalusta	A04	<Detection	6.03 ± 0.50	<Detection	0.006 ± 0.001	na	na
Gibeon 'Railway'	A03	0.06 ± 0.01	0.58 ± 0.19	0.001 ± 0.001	0.002 ± 0.002	na	na
Gibeon 'Egg'	G01a	5.20 ± 0.29	24.2 ± 1.4	0.09 ± 0.02	0.454 ± 0.030	270 ± 49	0.21 ± 0.02
Gibeon 'Egg'	G01b	5.56 ± 0.37	26.0 ± 1.7	0.10 ± 0.021	0.434 ± 0.031	250 ± 55	0.21 ± 0.02
Gibeon '99'	C06	1.61 ± 0.10	18.3 ± 1.2	0.06 ± 0.01	0.338 ± 0.028	300 ± 73	0.088 ± 0.008
IIG irons							
Tombigbee River	K04	3.34 ± 0.36	21.4 ± 1.3	0.08 ± 0.02	0.421 ± 0.031	270 ± 54	0.16 ± 0.02
Twannberg	C01	4.90 ± 0.28	23.4 ± 1.4	0.09 ± 0.02	0.483 ± 0.035	270 ± 51	0.21 ± 0.02
Ungrouped irons							
Chinga	M01	5.23 ± 0.35	23.8 ± 1.6	0.08 ± 0.02	0.400 ± 0.032	310 ± 85	0.22 ± 0.02
Mbosi	M02	0.032 ± 0.007	0.2 ± 0.1	<Detection	0.005 ± 0.003	na	na
Tishomingo	C02	43.6 ± 2.5	198 ± 11	0.71 ± 0.10	na	280 ± 42	0.22 ± 0.02

Table 2
Tungsten isotope compositions for the terrestrial standards analysed in this study.

	MC-ICPMS	N	$\varepsilon^{182/183}W$ $(6/3)_{meas.}$[a] $\pm 2\sigma$	$\varepsilon^{182/184}W$ $(6/4)_{meas.}$[a] $\pm 2\sigma$	$\varepsilon^{182/184}W$ $(6/3)_{meas.}$[a] $\pm 2\sigma$	$\varepsilon^{183}W$ $(6/4)_{meas.}$[a] $\pm 2\sigma$	$\varepsilon^{184}W$ $(6/3)_{meas.}$[a] $\pm 2\sigma$	$\varepsilon^{182/183}W$ $(6/3)_{corr.}$[a]	$\varepsilon^{182/184}W$ $(6/4)_{corr.}$[a]	$\varepsilon^{182/184}W$ $(6/3)_{corr.}$[a]
NIST129c[b]										
A07[c]	Nu Plasma	5	0.11 ± 0.15	-0.05 ± 0.15	0.06 ± 0.15	-0.21 ± 0.10	-0.14 ± 0.07	-0.16 ± 0.21	-0.05 ± 0.15	-0.07 ± 0.17
B07[c]	Nu Plasma	5	0.11 ± 0.10	-0.11 ± 0.06	0.02 ± 0.04	-0.14 ± 0.05	-0.09 ± 0.03	-0.08 ± 0.12	-0.11 ± 0.06	-0.07 ± 0.05
C07[c]	Nu Plasma	5	0.15 ± 0.23	0.05 ± 0.09	0.09 ± 0.22	-0.07 ± 0.12	-0.05 ± 0.08	0.06 ± 0.28	0.05 ± 0.09	0.04 ± 0.23
D07[c]	Nu Plasma	5	0.16 ± 0.08	0.02 ± 0.08	0.09 ± 0.07	-0.10 ± 0.07	-0.07 ± 0.05	0.02 ± 0.13	0.02 ± 0.08	0.02 ± 0.09
E07[c]	Nu Plasma	4	0.27 ± 0.13	0.07 ± 0.07	0.17 ± 0.07	-0.16 ± 0.08	-0.10 ± 0.05	0.07 ± 0.16	0.07 ± 0.07	0.07 ± 0.09
F07[c]	Nu Plasma	4	0.16 ± 0.14	-0.05 ± 0.05	0.07 ± 0.09	-0.15 ± 0.09	-0.10 ± 0.06	-0.04 ± 0.19	-0.05 ± 0.05	-0.03 ± 0.11
Mean Nu Plasma ($\pm$2SD, $n = 6$)				-0.01 ± 0.14				-0.02 ± 0.18	-0.01 ± 0.14	-0.01 ± 0.12
NIST129c										
G07[c]	Neptune Plus	4	0.17 ± 0.07	0.04 ± 0.16	0.10 ± 0.10	-0.08 ± 0.13	-0.05 ± 0.09	0.06 ± 0.19	0.04 ± 0.16	0.05 ± 0.13
R09	Neptune Plus	2	-0.02 ± 0.12	-0.03 ± 0.09	-0.01 ± 0.11	0.03 ± 0.03	0.02 ± 0.02	-0.02 ± 0.12	-0.03 ± 0.09	-0.01 ± 0.11
M09	Neptune Plus	5	0.06 ± 0.08	0.04 ± 0.07	0.05 ± 0.06	-0.01 ± 0.06	0.00 ± 0.04	0.06 ± 0.08	0.04 ± 0.07	0.05 ± 0.06
L05[c]	Neptune Plus	3	0.25 ± 0.09	-0.01 ± 0.11	0.10 ± 0.12	-0.18 ± 0.04	-0.12 ± 0.03	0.02 ± 0.11	-0.01 ± 0.11	-0.01 ± 0.12
L06[c]	Neptune Plus	4	0.22 ± 0.06	-0.04 ± 0.06	0.10 ± 0.09	-0.19 ± 0.03	-0.12 ± 0.02	-0.03 ± 0.07	-0.04 ± 0.06	-0.02 ± 0.09
O02	Neptune Plus	3	0.05 ± 0.10	0.08 ± 0.14	0.06 ± 0.12	0.01 ± 0.09	0.00 ± 0.06	0.05 ± 0.10	0.08 ± 0.14	0.06 ± 0.12
O03[c]	Neptune Plus	2	0.21 ± 0.06	0.04 ± 0.20	0.13 ± 0.15	-0.10 ± 0.21	-0.07 ± 0.14	0.07 ± 0.29	0.04 ± 0.20	0.06 ± 0.20
P09[c]	Neptune Plus	3	0.18 ± 0.12	0.05 ± 0.12	0.13 ± 0.12	-0.08 ± 0.04	-0.05 ± 0.03	0.08 ± 0.13	0.05 ± 0.12	0.08 ± 0.12
S04	Neptune Plus	5	0.02 ± 0.07	0.01 ± 0.05	0.01 ± 0.05	-0.01 ± 0.04	-0.01 ± 0.03	0.02 ± 0.07	0.01 ± 0.05	0.01 ± 0.05
Mean Neptune Plus ($\pm$2SD, $n = 9$)				0.02 ± 0.08				0.03 ± 0.08	0.02 ± 0.08	0.03 ± 0.08
Mean NIST129c All ($\pm$2SD, $n = 15$)				0.01 ± 0.10				0.01 ± 0.13	0.01 ± 0.10	0.01 ± 0.10
Alfa Aesar solution standard[d]	Neptune Plus	5	0.22 ± 0.06	-0.04 ± 0.06	0.10 ± 0.09	-0.19 ± 0.03	-0.12 ± 0.02	-0.03 ± 0.07	-0.04 ± 0.06	-0.02 ± 0.09
NIST3163 solution standard	Neptune Plus	5	0.01 ± 0.03	-0.02 ± 0.03	0.00 ± 0.03	-0.01 ± 0.03	-0.01 ± 0.02	0.01 ± 0.03	-0.02 ± 0.03	0.00 ± 0.03

[a] Normalized to $^{186}W/^{184}W = 0.92767$ (6/4) or $^{186}W/^{183}W = 1.9859$ (6/3) using the exponential law.
[b] High sulphur steel (NIST129c) doped with additional W to match concentrations of samples and subsequently processed through full chemical separation.
[c] Affected by and corrected for mass-independent effect (Section 4.2).
[d] Alfa Aesar solution standard processed through full chemical separation.

Table 3
W isotope compositions of iron meteorites investigated in this study.

Meteorite	ID	Source	N[b]	$\varepsilon^{182/183}W$ $(6/3)_{meas.}$[a] $\pm 2\sigma$	$\varepsilon^{182/184}W$ $(6/4)_{meas.}$[a] $\pm 2\sigma$	$\varepsilon^{182/184}W$ $(6/3)_{meas.}$[a] $\pm 2\sigma$	$\varepsilon^{183/184}W$ $(6/4)_{meas.}$[a] $\pm 2\sigma$	$\varepsilon^{183/184}W$ $(6/3)_{meas.}$[a] $\pm 2\sigma$	MC-ICPMS[d]	$\varepsilon^{182/183}W$ $(6/3)_{corr.}$[a] $\pm 2\sigma$	$\varepsilon^{182/184}W$ $(6/4)_{corr.}$[a] $\pm 2\sigma$	$\varepsilon^{182/184}W$ $(6/3)_{corr.}$[a] $\pm 2\sigma$
Low exposure age (<60 Myr) and/or effective shielding												
IIAB irons												
Edmonton, Canada[c]	A02	Univ. Alberta	10	−3.29 ± 0.08	−3.38 ± 0.07	−3.34 ± 0.07	−0.08 ± 0.05	−0.05 ± 0.03	Nept.	−3.39 ± 0.10	−3.38 ± 0.07	−3.39 ± 0.08
Braunau[c]	M03	Vienna	9	−3.22 ± 0.07	−3.40 ± 0.05	−3.31 ± 0.04	−0.13 ± 0.05	−0.09 ± 0.03	Nu	−3.40 ± 0.09	−3.40 ± 0.05	−3.40 ± 0.05
Mean IIAB irons					−3.39 ± 0.08					−3.39 ± 0.08	−3.39 ± 0.08	−3.40 ± 0.08
IIIAB irons												
Cape York 'CY01'[c]	A01	UC San Diego	8	−3.22 ± 0.11	−3.36 ± 0.12	−3.29 ± 0.11	−0.14 ± 0.04	−0.09 ± 0.03	Nu	−3.40 ± 0.12	−3.36 ± 0.12	−3.38 ± 0.11
Cape York 'CY02'[c]	G02	JNMC Zurich	3	−3.24 ± 0.05	−3.39 ± 0.17	−3.34 ± 0.06	−0.09 ± 0.14	−0.06 ± 0.09	Nept.	−3.36 ± 0.19	−3.39 ± 0.17	−3.40 ± 0.11
Mean IIIAB irons					−3.37 ± 0.10					−3.38 ± 0.18	−3.37 ± 0.14	−3.39 ± 0.12
IVA irons												
Gibeon '102'	C04/N02	Tokyo	4	−3.22 ± 0.15	−3.31 ± 0.08	−3.22 ± 0.10	−0.02 ± 0.10	−0.01 ± 0.07	Nept.	−3.22 ± 0.15	−3.31 ± 0.08	−3.22 ± 0.10
Gibeon 'Railway'[c]	A03/S01	Senckenberg	5	−3.19 ± 0.07	−3.42 ± 0.08	−3.30 ± 0.09	−0.17 ± 0.06	−0.11 ± 0.04	Nept.	−3.41 ± 0.11	−3.42 ± 0.08	−3.41 ± 0.10
Muonionalusta[c]	A04/S03	ETH IR-16	5	−3.23 ± 0.03	−3.33 ± 0.07	−3.29 ± 0.07	−0.08 ± 0.05	−0.05 ± 0.03	Nept.	−3.33 ± 0.07	−3.33 ± 0.07	−3.34 ± 0.07
Mean IVA irons (excl. Gibeon 'Railway')					−3.32 ± 0.08					−3.28 ± 0.08	−3.32 ± 0.08	−3.28 ± 0.08
Ungrouped irons												
Chinga[c,e]	M01	ETH IR-54	4	−3.21 ± 0.10	−2.86 ± 0.13	−3.04 ± 0.10	0.26 ± 0.09	0.17 ± 0.08	Nept.	−3.30 ± 0.10	−3.30 ± 0.17	−3.29 ± 0.14
Mbosi	M02	Senckenberg	4	−3.05 ± 0.10	−3.09 ± 0.03	−3.06 ± 0.07	−0.04 ± 0.08	−0.03 ± 0.05	Nept.	−3.05 ± 0.10	−3.09 ± 0.03	−3.06 ± 0.07
Higher exposure age (>100 Myr) and/or lower shielding												
IIAB												
Sikhote Alin 'SA01'	B01	ETH IR-27	7	−3.69 ± 0.16	−3.58 ± 0.24	−3.61 ± 0.16	0.08 ± 0.28	0.06 + 0.18	Nu	−3.69 ± 0.16	−3.58 ± 0.24	−3.61 ± 0.16
Mbosi	M02	Senckenberg	4	−3.05 ± 0.10	−3.09 ± 0.03	−3.06 ± 0.07	−0.04 ± 0.08	−0.03 ± 0.05	Nept.	−3.05 ± 0.10	−3.09 ± 0.03	−3.06 ± 0.07
IIAB												
Sikhote Alin 'SA02'[c]	G03	JNMC Zurich	2	−3.71 ± 0.14	−3.80 ± 0.12	−3.76 ± 0.11	−0.05 ± 0.13	−0.03 + 0.08	Nept.	−3.77 ± 0.21	−3.80 ± 0.12	−3.79 ± 0.14
Mbosi	M02	Senckenberg	4	−3.05 ± 0.10	−3.09 ± 0.03	−3.06 ± 0.07	−0.04 ± 0.08	−0.03 ± 0.05	Nept.	−3.05 ± 0.10	−3.09 ± 0.03	−3.06 ± 0.07
IIG												
Tombigbee River[c]	K04	AMNH	2	−3.38 ± 0.08	−3.60 ± 0.08	−3.50 ± 0.09	−0.16 ± 0.04	−0.11 + 0.02	Nept.	−3.60 ± 0.09	−3.60 ± 0.08	−3.61 ± 0.09
IVA												
Gibeon 'Egg'[c]	G01/S02	JNMC Zurich	5	−3.38 ± 0.13	−3.44 ± 0.09	−3.40 ± 0.06	−0.05 ± 0.10	−0.04 ± 0.07	Nept.	−3.45 ± 0.19	−3.44 ± 0.09	−3.44 ± 0.09
IVA												
Gibeon '99'[c]	C06	Tokyo	6	−3.50 ± 0.22	−3.63 ± 0.20	−3.59 ± 0.22	−0.04 ± 0.16	−0.03 + 0.11	Nu	−3.56 ± 0.31	−3.63 ± 0.20	−3.62 ± 0.25

All W isotope compositions are reported as ε-unit deviations relative to the bracketing solution standard (Alfa Aesar): $((^{18i}W/^{18j}W)_{sample}/(^{18i}W/^{18j}W)_{standard} - 1) \times 10^4$.
Uncertainties represent 95% confidence limits of the mean and are calculated using $(SD \times t_{0.95,N-1})/\sqrt{N}$ if $N > 4$.
For samples where $N < 4$ the uncertainty was estimated using the average 2SD of multiple analyses of the terrestrial metal standard (NIST129c) during the same session.

[a] Corrected for instrumental mass bias through internal normalisation to $^{186}W/^{183}W$ ('6/3') or $^{186}W/^{184}W$ ('6/4') using the exponential law.
[b] N = number of solution replicates.
[c] Affected by and corrected ('corr') for mass-independent effect (Section 5.2).
[d] MC-ICPMS used; 'Nu Plasma': Nu Instruments Plasma MC-ICPMS (ETH Zürich); 'Neptune Plus': ThermoScientific Neptune *Plus* MC-ICPMS (University of Münster).
[e] Corrected for *s*-process deficits using Arlandini et al. (1999) and the relations described in Burkhardt et al. (2012).

relations between measured He and Ne isotope concentrations and gas amounts that have been determined in dilution series experiments.

Blanks were measured with the same extraction and purification protocol as that used for the samples. At least one blank was measured after each sample. Subtracted blank signals are the average of multiple blanks ($n = 25$). For the He isotopes blanks were subtracted directly from raw signals. Measured Ne and Ar isotope signals were first corrected for trapped atmospheric noble gases using a two-component de-convolution based on assumed atmospheric and cosmogenic noble gas isotope ratios ($^{20}Ne/^{22}Ne_{COS} = 0.83$; $^{21}Ne/^{22}Ne_{COS} = 1$; $^{36}Ar/^{38}Ar_{COS} = 0.65$, $^{36}Ar/^{38}Ar_{ATM} = 5.32$) (Wieler, 2002). Cosmogenic ^{21}Ne and ^{38}Ar amounts were subsequently corrected for average cosmogenic contributions in the blanks, stemming from previous samples.

Reported external uncertainties (1SD) of cosmogenic noble gas concentrations represent the combined uncertainties of calibration, blank and sample measurements, together with the uncertainties involved in correcting for non-linear effects. For most of the samples these uncertainties are ~5–10% for ^{4}He, 5–10% for ^{3}He, 4–25% for $^{21}Ne_c$, and 6–10% for $^{38}Ar_c$. However, some noble gas concentrations that barely exceed background levels, and thus required large relative blank subtractions, have much larger uncertainties approaching ~100% (Table 1). Therefore, $^{4}He/^{21}Ne$ ratios are only reported in Table 1 if their uncertainties do not exceed 30% (1SD).

3.3. Tungsten isotope analyses

3.3.1. Sample preparation and chemical separation of W

Samples of ~0.5–1 g from all selected specimens were cut using a hand saw, thoroughly cleaned with abrasive paper followed by ethanol and de-ionised water in an ultrasonic bath. The outermost 15–25% of each sample were removed by leaching in 6 M HCl–0.06 M HF and a few drops of concentrated HNO_3 on a hotplate (90–110 °C) for 20–30 min. Complete dissolution of the samples was accomplished in ~15 ml 6 M HCl–0.06 M HF in Savillex® vials at 130 °C on a hotplate overnight. After complete dissolution, ~5% solution aliquots were taken to determine Hf and W concentrations by isotope dilution using a mixed ^{180}Hf–^{183}W isotope tracer (Kleine et al., 2004). As expected, all samples are virtually free of Hf and have $^{180}Hf/^{184}W$ lower than $\sim 8 \times 10^{-4}$.

Tungsten was separated from the sample matrix using a modified two-stage anion exchange chromatography after Horan et al. (1998) and Kleine et al. (2002, 2005a). The samples were loaded onto pre-cleaned anion exchange columns (4 ml BioRad® AG1X8, 200–400 mesh size) in 75 ml 0.5 M HCl–0.5 M HF. Most of the Fe–Ni matrix was washed off using 0.5 M HCl–0.5 M HF, and W was eluted in 15 ml 6 M HCl–1 M HF. After the first chemical separation, samples were dried down in HNO_3–H_2O_2 several times, and were then re-dissolved in 5 ml 0.5 M HCl–0.5 M HF. The second anion exchange chromatography is similar to the first-stage separation, but uses one instead of 4 ml anion exchange resin and includes an additional elution step (8 M HCl–0.01 M HF) that rinses off other trace elements (e.g., Ag). This step was found to be necessary when analysing the terrestrial metal standard (high-sulphur steel NIST 129c), which contains significant amounts of Ag. Silver, together with Ar and Cl, may form molecular interferences in the W mass range, as verified by isotope measurements of the W standard with admixed Ag. Magmatic iron meteorites contain too little Ag to significantly affect the W isotope analyses, however. Nevertheless, for direct comparison to the terrestrial standard, all samples were processed through the exact same chemical purification procedure. After the second chromatographic step, the W cuts were dried again, treated with HNO_3–H_2O_2 several times, and finally dissolved in a running solution (0.56 M HNO_3–0.24 M HF) yielding analyte W concentrations of 100 ppb (Nu Plasma) or 40–100 ppb (Neptune). The combined W yield for the two-stage chemistry was typically ~60–80%. Total procedural blanks varied between ~30 and 130 pg W and no blank corrections were necessary, given that ~150–400 ng W were analysed for each sample.

3.3.2. Tungsten isotope measurements

Tungsten isotope compositions were measured on a Nu Plasma MC-ICPMS at ETH Zürich following previously published procedures (Kleine et al., 2008) and on a ThermoScientific Neptune *Plus* MC-ICPMS at the Westfälische Wilhelms-Universität Münster. On both instruments, samples were introduced into the mass spectrometer using a Cetac Aridus II® desolvator. Standard Ni cones were used for all W isotope measurements (type B sampler + type A WA skimmer on the Nu Plasma; H cones on the Neptune *Plus*). Total ion beam intensities for W varied between 1 and 2×10^{-10} A at a 75 μL/min uptake rate (Nu Plasma, 100 ppb W) and were 1.5–5×10^{-10} A at a 50–100 μL/min uptake rate (Neptune *Plus*, 40–100 ppb W). Small isobaric interferences of Os on masses 184 and 186 were corrected by monitoring interference-free ^{188}Os. The Os interference corrections were generally smaller than 20 ppm and insignificant. Only Chinga (UNG) required a larger interference correction of ~3 ε-units. Instrumental mass bias was corrected normalising to either $^{186}W/^{183}W = 1.9859$ or $^{186}W/^{184}W = 0.92767$ and using the exponential law.

The $^{182}W/^{184}W$ and $^{183}W/^{184}W$ of the samples were measured relative to a terrestrial solution standard prepared from pure W metal (Alfa Aesar; Kleine et al., 2002, 2004). Tungsten isotope composition measurements consisted of 40 cycles of 5 s (Nu Plasma), or 200 cycles of 4.2 s integration time (Neptune *Plus*). Each measurement was bracketed by analyses of the Alfa Aesar solution standard. Baselines were measured by deflecting the ion beam using the electrostatic analyser (ESA) for 60–120 s. For analyses with relatively low ion beam intensities, baselines were determined on-peak using an acid blank solution (0.56 M HNO_3–0.24 M HF). Both methods proved to yield identical results. A 3–5 min washout using 0.56 M HNO_3–0.24 M HF between two successive measurements was sufficient to clean the sample introduction system.

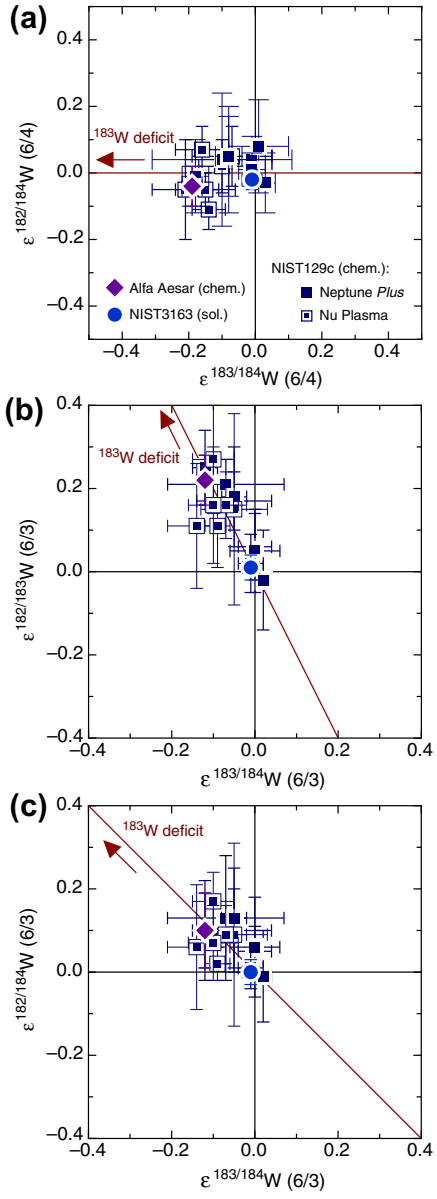

Fig. 1. Measured W isotope compositions for the terrestrial metal standard (NIST129c) relative to bracketing analyses of the solution standard (Alfa Aesar). (a) $\varepsilon^{182/184}$W (6/4) vs. $\varepsilon^{183/184}$W (6/4), (b) $\varepsilon^{182/183}$W (6/3) vs. $\varepsilon^{183/184}$W (6/3), and (c) $\varepsilon^{182/184}$W (6/3) vs. $\varepsilon^{183/184}$W (6/3), where '6/3' indicates that measured W isotope ratios were corrected for instrumental mass bias by internal normalisation using ^{186}W/^{183}W, and '6/4' by normalisation to ^{186}W/^{184}W. Also shown is the expected correlation line for a deficit in ^{183}W. Each data point represents multiple solution replicates ($n = 2$–5) of a digestion that was processed through the full chemical separation. Distinguished are samples measured with the Nu Plasma and ThermoScientific Neptune *Plus* MC-ICPMS. Also shown are the W isotope data for one aliquot of the Alfa Aesar solution standard that was processed through the full chemical separation (purple diamond), and for the NIST 3163 solution standard, which was not processed through the chemical separation (blue circle). Uncertainties are 95% conf. limits of the mean. Although the uncertainties of ε^{182}W and ε^{183}W (6/i) are correlated, error ellipses were omitted in this diagram for clarity. (For interpretation of the references to colour in this figure legend, the reader is referred to the web version of this article.)

Measured ^{182}W/^{184}W and ^{183}W/^{184}W ratios of samples are reported as ε-unit (i.e., parts per 10^4) deviations relative to the bracketing standard analyses. Reported are mean ε^{182}W and ε^{183}W values of pooled solution replicates ($n = 2$–9) at an external reproducibility of <0.2 ε-units (95% confidence limits of the mean) in most cases. The accuracy of the measurements was investigated through analysis of a terrestrial standard (high sulphur steel NIST129c) that was processed through the same purification procedure as the iron meteorite samples. Also, alternative isotope ratios (^{182}W/^{183}W and ^{182}W/^{184}W) and normalisation ratios for instrumental mass bias correction (^{186}W/^{183}W, '6/3' and ^{186}W/^{184}W, '6/4') were monitored and are used to assess possible matrix effects or artefacts.

4. RESULTS

4.1. Cosmogenic noble gases

The cosmogenic noble gas concentrations for the samples from this study are presented in Table 1. As anticipated, cosmogenic noble gas concentrations (index 'c') in most samples were found to be near the low end of the range observed in iron meteorites (Schultz and Franke, 2004). About half of the samples analysed here have ^{21}Ne$_c$ concentrations below $<0.01 \times 10^{-8}$ cm^{3}STP/g, while another group of samples shows slightly higher ^{21}Ne$_c$ values between 0.01 and 0.7×10^{-8} cm^{3}STP/g. In contrast, one of the Sikhote Alin samples (SA01) contains $\sim 2.6 \times 10^{-8}$ cm^{3}STP/g of ^{21}Ne$_c$. Since cosmogenic ^{22}Ne cannot be determined directly we cannot discuss cosmogenic ^{22}Ne/^{21}Ne ratios and, therefore, cannot correct the ^{21}Ne$_c$ concentrations for contributions from possible phosphorous and/or sulphur inclusions. This might in principle somewhat compromise the quality of the ^{21}Ne$_c$ data and the discussion of pre-atmospheric sizes and exposure ages. However, given the consistency of the dataset (see below), we consider any contributions to ^{21}Ne$_c$ from sulphur and/or phosphorus inclusions to be small for the meteorites studied here.

4.2. Tungsten isotopes

4.2.1. Terrestrial standard

The W isotopic data for the terrestrial standard (NIST129c) are provided in Table 2 and Figs. 1 and 2. The ε^{18i}W values are given for different W isotope ratios (^{182}W/^{183}W, ^{182}W/^{184}W, ^{183}W/^{184}W) and for different normalising ratios (^{186}W/^{183}W or ^{186}W/^{184}W, subsequently marked as '(6/3)' and '(6/4)', respectively). All eight measurements for NIST 129c – each of which represents the average of 2–5 measurements of a single sample that was processed through the full chemical separation – show small but resolved positive $\varepsilon^{182/183}$W (6/3) (up to +0.27) and negative $\varepsilon^{183/184}$W (6/3) (down to −0.14) anomalies. These effects are observed for measurements performed both on the Neptune *Plus* (WWU Münster) and on the Nu Plasma MC-ICPMS (ETH Zürich). The average of all eight measurements of the NIST129c standard yields mean $\varepsilon^{182/183}$W (6/3) $= +0.14 \pm 0.05$, $\varepsilon^{182/184}$W (6/3) $= +0.08 \pm 0.03$, and $\varepsilon^{183/184}$W (6/4) $= -0.10 \pm 0.04$ (SE 95% conf., $n = 15$).

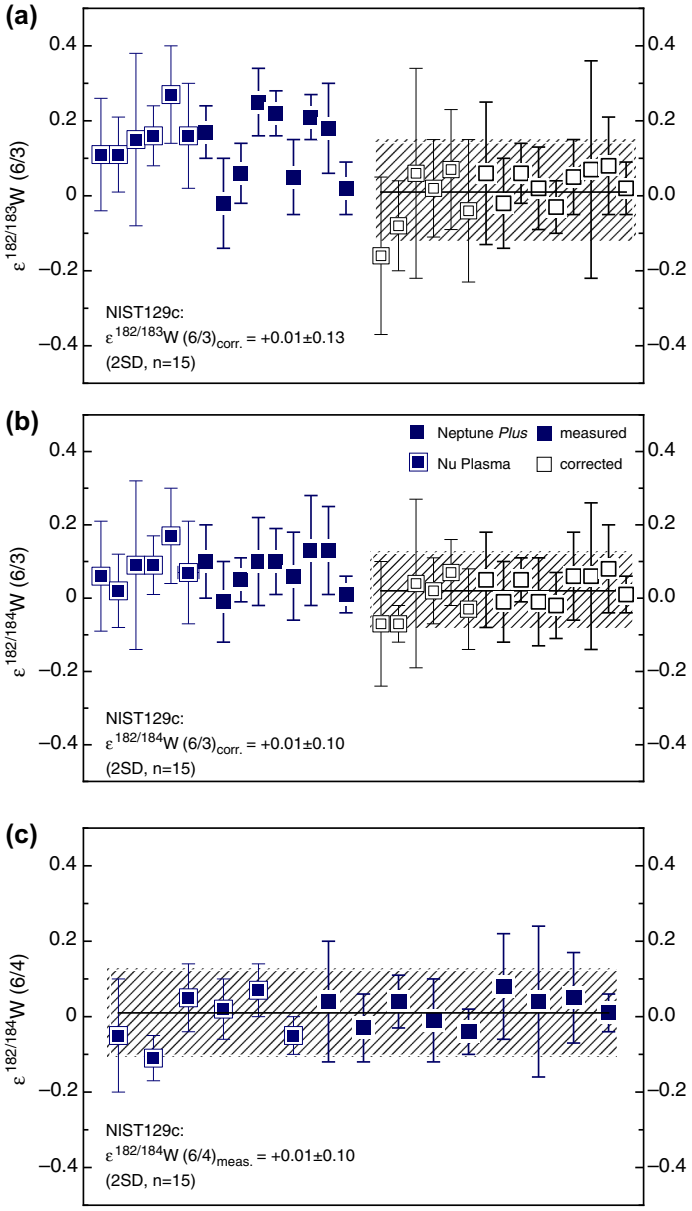

Fig. 2. External reproducibility of $\varepsilon^{182}W$ for the terrestrial metal standard (NIST129c). (a) $\varepsilon^{182/183}W$ (6/3), (b) $\varepsilon^{182/184}W$ (6/3), and (c) $\varepsilon^{182/184}W$ (6/4). Each data point represents multiple solution replicates ($n = 2$–5) of a digestion that was processed through the full chemical separation. For normalizations involving ^{183}W (i.e., those that are potentially affected by a mass-independent effect), both the corrected and uncorrected $\varepsilon^{182}W$ values are shown. Error bars on individual data points are 95% conf. limits of the mean. The hashed area shows the external reproducibility of the NIST129c standard analyses (2SD).

Thus, while both $^{182}W/^{183}W$ (6/3) and $^{182}W/^{184}W$ (6/3) values are elevated, the $^{183}W/^{184}W$ ratio is lower than that of the solution standard. The anomaly in $\varepsilon^{182/183}W$ (6/3) is twice that in $\varepsilon^{183/184}W$ (6/3), while the anomalies in $\varepsilon^{182/184}W$ (6/3) and $\varepsilon^{183/184}W$ (6/3) are identical. At the same time no anomaly is apparent in $\varepsilon^{182/184}W$ (6/4) with an average value identical to zero ($\varepsilon^{182/184}W$ (6/4) $= 0.01 \pm 0.10$, 2SD, $n = 15$). Thus, only W isotope ratios involving ^{183}W yield inaccurate results, while the $^{182}W/^{184}W$ ratio (6/4) is not affected. This indicates that the slight offset observed for the NIST129c data is caused by a mass-independent W isotope fractionation of the odd isotope ^{183}W from the even isotopes ^{182}W, ^{184}W and ^{186}W. The same negatively correlated shifts in $\varepsilon^{182/184}W$ (6/3) and $\varepsilon^{183/184}W$ (6/3) relative to the unprocessed solution standard have been observed by Willbold et al. (2011) for W isotope measurements on terrestrial silicate samples.

The observed ^{183}W isotope effect in the terrestrial metal standard may reflect an anomalous isotope composition of the bracketing solution standard (i.e., Alfa Aesar) relative to the true terrestrial composition. However, an aliquot of the Alfa Aesar solution standard passed through the full chemical separation produced identical anomalies to those observed for the metal standard (NIST129c) (Fig. 1

and Table 2). Furthermore, another solution standard (NIST3163) yields a W isotope composition identical to that of the Alfa Aesar standard (Fig. 1). An anomalous W isotope composition of the Alfa Aesar solution standard, therefore, cannot be the cause of the mass-independent ^{183}W effect observed for the NIST 129c metal standard. This effect must rather be related to processes during sample preparation and W purification and we concur with Willbold et al. (2011) that a mass-independent isotope fractionation between odd (i.e., ^{183}W) and even W isotopes (i.e., ^{182}W, ^{184}W and ^{186}W) associated with W-loss during re-dissolution of purified W in Savillex vials is causing the observed ^{183}W deficits.

The mass-independent ^{183}W effect on terrestrial standards and meteorite samples can be corrected by using different normalisation schemes for the W isotope measurements. For example, the terrestrial metal standards analysed in this study plot on a line with a slope of ~−2 that is predicted for ^{183}W deficits in $\varepsilon^{182/183}$W (6/3) vs. $\varepsilon^{183/184}$W (6/3) space (Fig. 1b). Likewise, the data plot on a line of slope ~−1 in $\varepsilon^{182/184}$W (6/3) vs. $\varepsilon^{183/184}$W (6/3) space, again consistent with the predicted effect of a ^{183}W deficit (Fig. 1c). For all samples, measured $\varepsilon^{182/183}$W (6/3) and $\varepsilon^{182/184}$W (6/3) values can thus be corrected using the measured $\varepsilon^{183/184}$W (6/3) and the relations $\varepsilon^{182/183}\text{W}\ (6/3)_{\text{corr.}} = \varepsilon^{182/183}\text{W}\ (6/3)_{\text{meas.}} - (-2) \times \varepsilon^{183/184}\text{W}\ (6/3)$ and $\varepsilon^{182/184}\text{W}\ (6/3)_{\text{corr.}} = \varepsilon^{182/184}\text{W}\ \ (6/3)_{\text{meas.}} - (-1) \times \varepsilon^{183/184}\text{W}\ \ (6/3)$ (Table 2). The corrected $\varepsilon^{182/183}$W (6/3) and $\varepsilon^{182/184}$W (6/3) values are identical to the measured $\varepsilon^{182/184}$W (6/4), indicating that the corrections are accurate (Fig. 2).

4.2.2. Iron meteorites

Tungsten isotope compositions for the iron meteorite samples are displayed in Table 3 and Figs. 3 and 4. The co-variation of $\varepsilon^{182/184}$W (6/3) and $\varepsilon^{183/184}$W (6/3) measured for the iron meteorites (Fig. 3) is similar to the correlated effects observed for the terrestrial metal standard (NIST129c) (Fig. 1). While many of the samples analysed here have $\varepsilon^{183/184}$W indistinguishable from the terrestrial value (i.e., the Alfa Aesar solution standard), about half of the samples exhibit small $\varepsilon^{183/184}$W deviations that are resolved from the terrestrial value. These samples also show differences of similar magnitude in their ε^{182}W values calculated using different normalisation schemes (Fig. 3).

For all iron meteorite samples investigated here (except Chinga) the difference between $\varepsilon^{182/184}$W (6/3) and $\varepsilon^{182/184}$W (6/4) is identical to the negative anomaly observed for ε^{183}W (6/3) (Table 3). Similarly, the difference between $\varepsilon^{182/183}$W (6/3) and $\varepsilon^{182/184}$W (6/4) corresponds to twice the anomaly observed for ε^{183}W (6/3). These systematic W isotope shifts are the same as those observed for the NIST129c standard, and are also in agreement with the predicted effects for a deficit in ^{183}W (Fig. 3). This strongly suggests that the observed mass-independent ^{183}W effects in the NIST129c data and the iron meteorite samples have the same origin. The iron meteorite data can thus be corrected using the same approach employed above for the NIST129c standard. The corrected $\varepsilon^{182/184}$W (6/3) and $\varepsilon^{182/183}$W (6/3) values are shown in Table 3, and are in excellent agreement with the $\varepsilon^{182/184}$W (6/4) values directly measured for the iron meteorites. This again demonstrates that, as for the NIST 129c data, the correction for the mass-independent ^{183}W effect is accurate. We nevertheless emphasise that the main conclusions of our study are not compromised by the mass-independent ^{183}W effect present in some of the sample measurements, because the chronological interpretation of the Hf–W data is entirely based on $\varepsilon^{182/184}$W (6/4) values (i.e., the W isotope ratio not involving ^{183}W), which do not show this effect and, hence, do not require any correction at all.

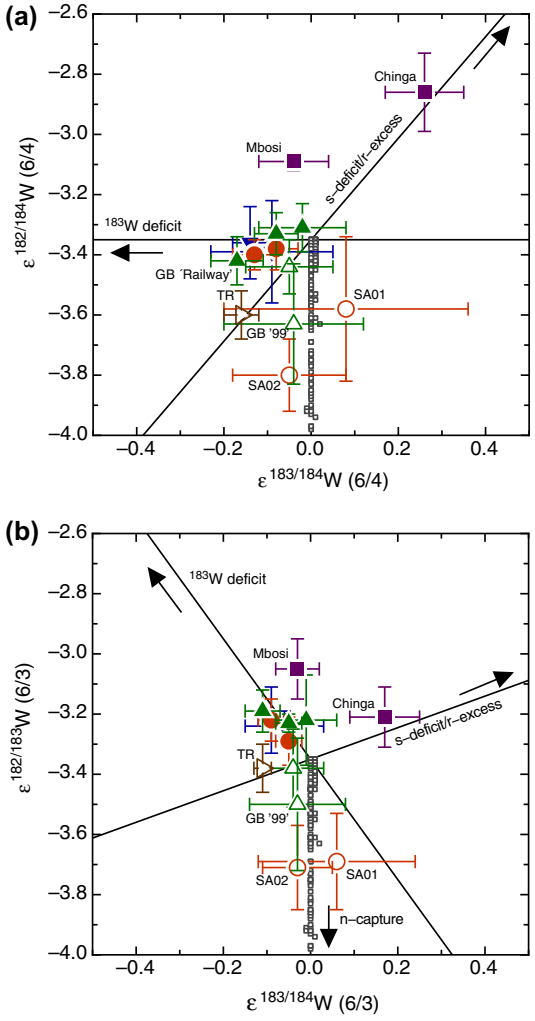

Fig. 3. ε^{182}W–ε^{183}W variation for iron meteorite samples analysed in this study: (a) $\varepsilon^{182/184}$W (6/4) vs. $\varepsilon^{183/184}$W (6/4), (b) $\varepsilon^{182/183}$W (6/3) vs. $\varepsilon^{183/184}$W (6/3). Error bars indicate 95% conf. limits of the mean ($n = 2$–9). Also shown are: (i) the expected correlation line for the mass-independent effect (i.e., a deficit in ^{183}W); (ii) the expected correlation line for variations in *s*- and *r*-process W isotopes calculated using the stellar model from Arlandini et al. (1999); and (iii) model arrays (small grey squares) for neutron capture effects on W isotopes in iron meteoroids. The solid lines intersect at an ordinate value of $\varepsilon^{182}\text{W} = -3.35$, which is approximately the average value for the investigated iron meteorites groups. Although the uncertainties of $\varepsilon^{182/i}$W and $\varepsilon^{183/184}$W (6/i) are positively correlated, error ellipses were omitted in this diagram for clarity.

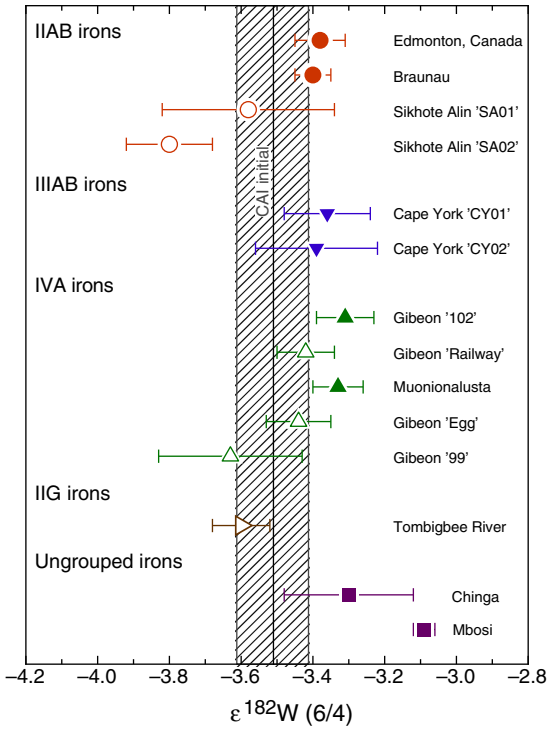

Fig. 4. $\varepsilon^{182/184}W$ (6/4) for the iron meteorite samples investigated in this study. Distinguished are samples with low exposure ages whose W isotope compositions are unaffected by cosmic ray effects (filled symbols) and samples which have longer exposure times and/or whose $\varepsilon^{182}W$ was lowered as a result of cosmic ray interactions (open symbols). For Chinga (UNG) the $\varepsilon^{182}W$ corrected for nucleosynthetic isotope anomalies is shown. The vertical hashed area represents the CAI initial of $\varepsilon^{182}W = -3.51 \pm 0.10$ (Burkhardt et al., 2008, 2012). Error bars indicate 95% conf. limits of the mean.

The iron meteorite samples from groups IIAB, IIIAB and IVA with the lowest noble gas concentrations display a narrow range of $\varepsilon^{182/184}W$ (6/4) values, from −3.42 to −3.31 (Table 3), slightly higher than the current best estimate for the initial W isotope composition of CAI [$\varepsilon^{182}W = -3.51 \pm 0.10$; Burkhardt et al. (2012)]. In general, samples with higher noble gas concentrations tend to have lower $\varepsilon^{182}W$ values (Tables 1 and 3). Among these samples, Sikhote Alin (IIAB, sample SA02) stands out by having $\varepsilon^{182}W$ significantly below the initial W isotope composition of CAI. The two ungrouped iron meteorites analysed here (Chinga and Mbosi) have $\varepsilon^{182}W$ significantly higher (up to ~0.4 ε-units) than those observed for samples from the major groups of investigated magmatic iron meteorites (Figs. 3 and 4; Table 3). One of the ungrouped iron meteorites (Chinga) stands out by also having a positive $\varepsilon^{183}W$ anomaly resolved from zero.

5. DISCUSSION

5.1. Identifying iron meteorite samples with very low fluences of (epi)thermal neutrons

Very low concentrations of cosmogenic noble gases in an iron meteorite sample may be the result of a low exposure age or of a heavily shielded location in a large meteoroid. In the first case, W isotope compositions will essentially be unaffected by cosmic rays irrespective of meteoroid size and sample position. A sample from a large meteoroid may also be unaffected by cosmic rays, regardless of its exposure age, if it was located deep enough in the pre-atmospheric body such that not only the high energy particle fluence but also the epi(thermal) neutron fluence were strongly attenuated. However, if a sample was irradiated at some intermediate depth where the high energy particle flux was already low but the (epi)thermal neutron flux was still high, noble gas concentrations in the sample may underestimate the modification of its W isotopic composition by neutron capture effects. Model calculations for neutron capture effects on W isotope compositions suggest that for a spherical iron meteoroid with an exposure age of 60 Ma, the maximum cosmic ray induced decrease in $\varepsilon^{182}W$ would be ~0.09 ε-units [calculated using the nuclide production model described for noble gases and several radionuclides by Ammon et al. (2009) and Leya and Masarik (2009)], which is close to our average analytical uncertainty (Tables 2 and 3). This maximum cosmogenic effect would be reached in the centre of an iron meteoroid with a radius of 85 cm. As for all other meteoroid sizes and sample depths the correction would be – partly considerably – smaller than 0.09 ε-units, we consider the measured W isotopic composition in meteorites with exposure ages <60 Ma unaffected by neutron capture effects. In the following paragraphs we therefore evaluate which of the meteorites studied here can be assigned exposure ages below 60 Ma (Table 4). We will, at this stage, assume that all samples were subjected to a single stage exposure history to cosmic rays, i.e., we assume that the entire fluence of (epi)thermal neutrons in any sample was acquired at the same shielding and over the same time interval as the entire fluence of the high energy particles producing cosmogenic noble gases. We will later discuss the validity of this assumption in light of the W isotope data. We furthermore assume a temporally constant primary cosmic ray flux (cf. Wieler et al., 2011).

Braunau (IIAB, 39 kg) has a shielding-corrected very low exposure age of approximately 8 Ma, determined with the cosmogenic nuclide pairs ^{39}Ar–^{38}Ar, ^{36}Cl–^{10}Be and ^{36}Cl–^{36}Ar, respectively (Cobb, 1966; Chang and Wänke, 1969). According to the model calculations by Ammon et al. (2009), the noble gas concentrations of the investigated sample (e.g., $^{21}Ne_c = 0.17$; $^{38}Ar_c = 0.65 \times 10^{-8}$ cm^3STP/g) indicate production rates as expected for a meteoroid with a radius of ⩽15 cm, consistent with the recovered mass of Braunau. The very low $^4He/^{21}Ne$ ratio of ~150, although not precise, also hints at a relatively small pre-atmospheric size. The low exposure age and small pre-atmospheric size indicate that the W isotope composition of Braunau certainly remained unaffected by cosmic ray effects. The maximum shift in $\varepsilon^{182}W$ predicted by our neutron capture model for a meteorite having $T_{CRE} = 8$ Ma corresponds to ~−0.01 ε-units (Table 4).

Cape York (IIIAB) is a large (>58,000 kg; pre-atmospheric radius >1.2 m) and well-studied iron meteorite. Our three noble gas analyses on samples from two different specimens (CY01 and CY02) yield similar concentrations at

Table 4
Summary of iron meteorite samples with minimal cosmic ray effects.

Meteorite	ID	Radius[a]	Cosmic-ray exposure age (T_{CRE})[b]		Max. $\Delta\varepsilon^{182}W_{GCR}$[c]	Measured $\varepsilon^{182}W$	Δt_{CAI}
		[cm]	[Ma]	Method	(model)	[±95% conf.]	[Myr]
IIAB irons							
Braunau	M03	⩽15	~8	^{39}Ar–^{38}Ar, ^{36}Cl–^{10}Be and ^{36}Cl–^{36}Ar (1)	⩽−0.01	−3.40 ± 0.05	
Edmonton, Canada	A02	<120	<60	Production rates (4)	⩽−0.09	−3.38 ± 0.07	
Mean IIAB						−3.39 ± 0.08	$+1.0^{+1.1}_{-1.0}$
IIIAB irons							
Cape York (CY01)	A01	⩾120	82 ± 7	^{129}I–^{129}Xe (2)	⩽−0.08	−3.36 ± 0.05	
Cape York (CY02)	G02a	⩾120	82 ± 7	^{129}I–^{129}Xe (2)	⩽−0.08	−3.39 ± 0.17	
Mean IIIAB						−3.37 ± 0.14	$+1.2^{+1.5}_{-1.4}$
IVA irons							
Gibeon '102'	C04	⩾90	<50	^{10}Be–^{21}Ne (3)	⩽−0.07	−3.31 ± 0.08	
Muonionalusta	A04	<120	<6	Production rates + noble gases (4)	⩽−0.01	−3.33 ± 0.07	
Gibeon 'Railway'	A03	⩾90	<50	^{10}Be–^{21}Ne (3)	⩽−0.07	−3.42 ± 0.08	
Mean IVA (excl. 'Railway')						−3.32 ± 0.08	$+1.6^{+1.1}_{-1.0}$
Ungrouped irons							
Chinga	M01	⩽60	<40	Production rates + noble gases (4)	⩽−0.05	−3.30 ± 0.17	$+1.8^{+1.8}_{-1.7}$
Mbosi	M02	<120	<6	Production rates + noble gases (4)	⩽−0.01	−3.09 ± 0.03	$+3.9^{+0.9}_{-0.9}$

Tombigbee River (IIG) is not shown as it likely had a complex exposure history and its W isotope composition was likely modified by cosmic rays (Section 5.3).

[a] Pre-atmospheric radius for a spherical meteoroid, based on either the total recovered mass (lower bound), or noble gas systematics (upper bound).

[b] Cosmic-ray exposure ages (or upper and lower bounds thereof) and the method(s) used for determining these ages. References: (1) Cobb (1966); Chang and Wänke (1969); (2) Mathew and Marti (2009); (3) Honda et al. (2009); (4) Ammon et al. (2009)/this study.

[c] Model prediction for maximum cosmic-ray effect on $\varepsilon^{182}W$ for given T_{CRE} (Ma), pre-atmospheric radius, and $^4He/^{21}Ne$ (if determined).

the very low end of the range of values observed in iron meteorites (Table 1), in agreement with other Cape York analyses (Schultz and Franke, 2004). A shielding corrected ^{129}I–^{129}Xe exposure age of 82 ± 7 Ma was determined by Mathew and Marti (2009), slightly higher than the 60 Ma limit mentioned above. However, according to the nuclide production model of Ammon et al. (2009) and Leya and Masarik (2009), in a $r = 1.2$ m meteoroid the maximum cosmic ray-induced decrease in $^{182}W/^{184}W$ for a 82 Ma exposure age is ~0.08 $\varepsilon^{182}W$, even marginally lower than the limit of 0.09 $\varepsilon^{182}W$ tolerated here. We therefore include Cape York into our set of 'low exposure age meteorites' (Table 4).

Gibeon (IVA) is a large iron meteorite (>26,000 kg; radius >0.9 m). Reported noble gas concentrations are variable, yet again near the low end of the range observed for iron meteorites (Schultz and Franke, 2004). The Gibeon samples analysed here also have varying noble gas concentrations (Table 1). In a comprehensive study, Honda et al. (2009) report shielding-corrected ^{21}Ne–^{10}Be cosmic ray exposure ages for a large number of Gibeon specimens. These authors identified two groups of samples, one with only loosely defined but low (~10–50 Ma) and another with high (~300 Ma) exposure ages. Honda et al. (2009) conclude that Gibeon had a complex exposure history. The samples with low nominal exposure ages (<50 Ma) thus presumably were largely shielded from highly energetic cosmic rays prior to their second (meteoroid) exposure stage and thus likely also had seen a considerably lower (epi)thermal neutron fluence than the samples of the other group. The ^{21}Ne analyses for Gibeon specimens '99', '102' and 'Railway' from Honda et al. (2009) are in agreement with our ^{21}Ne results for exactly these samples (Table 1). Honda et al. (2009) interpreted the samples 'Railway' and '102' to belong to the low exposure age group (<50 Ma). We thus expect cosmic ray effects on W isotopes to be minimal for these samples, assuming a low (epi)thermal neutron fluence for the two samples during the first exposure stage (i.e., for the low noble gas group the above assumption that the total fluences of high energy- and (epi)thermal particles were both acquired at the same constant shielding can be expected to be correct). The maximum negative shift in $\varepsilon^{182}W$ predicted by the neutron capture model for $T_{CRE} = 50$ Ma and $r > 0.9$ m corresponds to −0.07 ε-units. As minor – albeit not resolved – variations might thus be expected, the sample with the most elevated $\varepsilon^{182}W$, i.e., Gibeon '102', will be taken as representative for Gibeon before exposure to cosmic rays. The other two Gibeon samples analysed here ('Egg' and '99') have higher noble gas concentrations than the 'Railway' and '102' specimens. Although in absolute terms the concentrations of 'Egg' and '99' are still low, these two specimens supposedly belong to the second group recognised by Honda et al. (2009) with an exposure age of approximately 300 Ma. The W isotope compositions of these two samples may thus have been modified by cosmic ray effects.

No shielding-corrected exposure ages based on pairs of a radioactive and a stable cosmogenic nuclide are available for *Edmonton*, *Canada* (IIAB, pre-atmospheric mass >7 kg), *Muonionalusta* (IVA, >230 kg), *Tombigbee River* (IIG, >43 kg), *Chinga* (UNG, >200 kg), and *Mbosi* (UNG, >16,000 kg). However, it seems likely that all these meteorites owe their low noble gas concentrations primarily to a low exposure age rather than a very high shielding. For Tombigbee River and Chinga a rough maximum pre-atmospheric radius of ~60 cm (Ammon et al., 2009) can be estimated from the upper limit of the $^{4}He/^{21}Ne$ ratio of ~300 (Table 1). The minimum ^{21}Ne production rate in the centre of meteoroids of this radius is $\sim 0.19 \times 10^{-10}$ cm^3STP/g Ma (Ammon et al., 2009). This yields maximum one stage cosmic ray exposure ages of ~40 Ma for both Tombigbee River and Chinga. For Edmonton, the uncertainty of the $^{4}He/^{21}Ne$ ratio is too large to obtain an estimate of the maximum pre-atmospheric radius. However, assuming that the Edmonton sample originated from close to the centre of an iron meteoroid with a pre-atmospheric radius of 120 cm, which is the largest object modelled by Ammon et al. (2009), yields an maximum possible one stage exposure age of ~60 Ma. With the same assumption we arrive at upper limits of ~6 Ma for the exposure ages of Muonionalusta and Mbosi for which $^{21}Ne_{cos}$ was below detection limit, if we additionally assume these samples to have had a $^{21}Ne_{cos}$ concentration of 1×10^{-11} cm^3STP/g, i.e., the lowest value we were able to measure in one of our samples (Gibeon 'Railway'). Thus, for all these samples cosmic ray effects on W isotopes can be expected to be minimal and smaller than our analytical resolution for $^{182}W/^{184}W$.

Sikhote Alin (27,000 kg; radius >0.9 m) has a ^{40}K–K exposure age of 430 Ma (Voshage, 1984). Hence, Sikhote Alin is the only meteorite in this study with an unequivocally high exposure age. The samples investigated here (SA01 and SA02) presumably derive from rather near the surface of this large meteoroid, as suggested by their $^{4}He/^{21}Ne$ ratios of ~215 and 250 (Ammon et al., 2009). Also, sample SA01 has by far the highest noble gas concentrations observed in this study and even contains an order of magnitude more gas than the two SA02 samples. Significant cosmic ray effects on W isotopes can thus be anticipated in SA01 but possibly also in SA02.

In summary, the samples with shielding-corrected exposure ages <60 Ma as deduced by pairs of stable and radioactive nuclides [Braunau and Gibeon ('102' and 'Railway')], as well as Cape York with its 82 Ma exposure age are expected to have a W isotopic composition not modified by epi(thermal) neutron capture reactions beyond the present analytical uncertainty of ~0.1 ε ^{182}W (95% conf.), and any corrections should mostly be lower than this value (Table 4). Five other meteorites (Edmonton Canada, Muonionalusta, Tombigbee River, Chinga, and Mbosi) very likely also have low noble gas based exposure ages and hence should be expected to have W isotope compositions that are unaffected by cosmic rays within our current analytical resolution. We will discuss below, however, that Tombigbee River may have to be excluded from this group, because our assumption of a single stage exposure history to cosmic rays does not seem to be valid for this sample. The W isotope compositions of Sikhote Alin (samples SA01 and SA02), and possibly also Gibeon ('99' and 'Egg') will likely have been modified more strongly by neutron capture. We emphasise that for the following discussion we use only *measured* $^{182}W/^{184}W$, without any attempt to correct for neutron capture effects.

5.2. Core formation ages for samples with minimal cosmic ray effects

A model time of metal–silicate separation (i.e., core formation) in iron meteorite parent bodies can be calculated as the time of Hf–W fractionation from an unfractionated, chondritic reservoir. The model age of core formation is conveniently expressed as the time elapsed since formation of CAI and is calculated using the relation

$$\Delta t_{CAI} = -\frac{1}{\lambda} \ln \left\{ \frac{(\varepsilon^{182}W)_{Sample} - (\varepsilon^{182}W)_{Chondrites}}{(\varepsilon^{182}W)_{SSI} - (\varepsilon^{182}W)_{Chondrites}} \right\} \quad (1)$$

in which λ is the ^{182}Hf decay constant of 0.078 ± 0.002 Myr^{-1} (Vockenhuber et al., 2004), $\varepsilon^{182}W_{Chondrites}$ is the present-day $\varepsilon^{182}W$ of chondrites ($\varepsilon^{182}W = -1.9 \pm 0.1$) (Kleine et al., 2002, 2004; Schönberg et al., 2002; Yin et al., 2002), $\varepsilon^{182}W_{sample}$ is the $\varepsilon^{182}W$ value of an iron meteorite, and $\varepsilon^{182}W_{SSI}$ is the solar system initial W isotopic composition as determined from a Hf–W isochron for CAI (Burkhardt et al., 2008, 2012). The current best estimate for this value is $\varepsilon^{182}W_{SSI} = -3.51 \pm 0.10$ (Burkhardt et al., 2012). Note that this value is lower than that used previously (Burkhardt et al., 2008), as a result of correcting the CAI data for nucleosynthetic isotope anomalies (Burkhardt et al., 2012).

As pointed out in Section 5.1 the fluence of (epi)thermal neutrons is expected to have been minimal for many of the investigated samples. This applies to the meteorites that have shielding-corrected known low exposure ages (i.e., Braunau, Gibeon '102' and 'Railway', Cape York) as well as further samples with most likely low exposure ages (Edmonton Canada, Muonionalusta, Tombigbee River, Chinga, and Mbosi). The ungrouped irons Chinga and Mbosi will be discussed in Section 5.3. With the exception of Tombigbee River, all samples with low noble gas based exposure ages indeed show $\varepsilon^{182}W$ values identical to each other within our analytical resolution (i.e., ~0.1 ε units), and slightly higher than the initial W isotope composition of CAI (Fig. 4). In contrast, samples for which the noble gas systematics indicate exposure ages of several hundred Ma (i.e., Sikhote Alin, and the two Gibeon specimens '99' and 'Egg' with a discernible long first exposure stage) display more negative and more variable $\varepsilon^{182}W$ values. Sample SA02 from Sikhote Alin has a $\varepsilon^{182}W$ value significantly lower than the initial W isotope composition in CAI. Thus, the low values of both Sikhote Alin and the two Gibeon specimens '99' and 'Egg' are reasonably explained as the result of ^{182}W burnout resulting from cosmic ray-induced neutron capture reactions.

The only data point in Fig. 4 not perfectly fitting the overall picture is that of Tombigbee River, whose $\varepsilon^{182}W$ value is slightly lower than the CAI initial and significantly

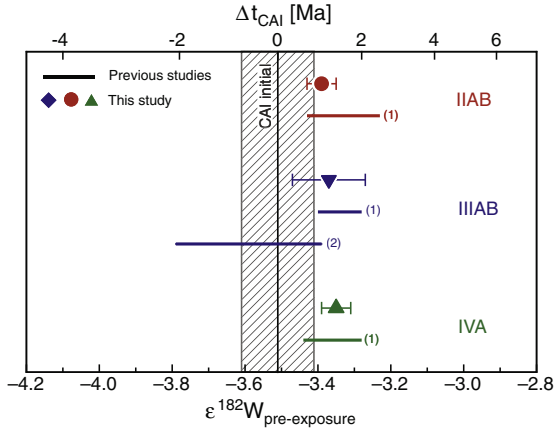

Fig. 5. Mean $\varepsilon^{182}W$ for samples with low cosmic ray exposure ages for the IIAB, IIIAB, IVA iron meteorite groups. The upper axis shows the timing of core formation relative to the formation of CAI [i.e., $\varepsilon^{182}W = -3.51 \pm 0.10$; (Burkhardt et al., 2008, 2012)]. Shown for comparison are the corrected $\varepsilon^{182}W$ values obtained in previous studies that employed cosmogenic noble gas systematics or theoretical models of more strongly irradiated meteorites to correct for cosmic ray effects (2: Markowski et al., 2006a; 1: Qin et al., 2008b). Note that the uncertainty on the initial W isotope composition of CAI is excluded from the error bars on the calculated ages, but instead is shown separately (hashed area).

lower than values of any other sample for which the noble gas systematics indicate a low exposure age. Complex exposure histories are not uncommon among iron meteorites (e.g., Welten et al., 2008). One explanation for this discrepancy, therefore, is that – contrary to our assumption in Section 5.1 – Tombigbee River had a complex irradiation history, shielded in a first stage deeply enough to have seen only a relatively small fluence of high-energy cosmic ray particles but discernible amounts of (epi)thermal neutrons. However, for all other samples for which cosmic ray effects on W isotopes are expected to be minimal, the perfect consistency between W isotopic data on the one hand and cosmogenic noble gas or radionuclide data on the other strongly indicates that our basic assumption here is valid: samples identified as having a low cosmic ray exposure age have experienced a negligible fluence of (epi)thermal neutrons. Among our low exposure age group of meteorites, Tombigbee River thus appears to be the only meteorite with a complex exposure history.

The mean $\varepsilon^{182/184}W$ (6/4) values of the investigated iron meteorite samples with low exposure ages and negligible cosmic ray effects are -3.39 ± 0.08, -3.37 ± 0.14, and -3.32 ± 0.08 (±95% conf.) for the IIAB, IIIAB, and IVA iron meteorite groups (Tables 3 and 4; Fig. 5). These values are in excellent agreement with results from a previous study that used theoretical models and noble gas systematics to correct for cosmic ray-induced effects (i.e., IIAB: -3.30 ± 0.10; IIIAB: -3.34 ± 0.06; IVA: -3.36 ± 0.07; Fig. 5; Qin et al., 2008b), indicating that this procedure quantitatively corrected for the effects of ^{182}W burnout in the IIAB, IIIAB and IVA iron meteorites. Nevertheless, in contrast to the samples investigated in previous studies, the weakly irradiated samples identified here require no correction for cosmic ray effects on their W isotopic compositions. As such, these samples are of paramount importance to establish a precise Hf–W chronometry of iron meteorites.

Core formation ages deduced from the *measured* $\varepsilon^{182}W$ values of the IIAB, IIIAB, and IVA irons having negligible cosmic ray effects are displayed in Fig. 5. The core formation ages, calculated relative to a solar system initial $\varepsilon^{182}W = -3.51 \pm 0.10$ (Burkhardt et al., 2012), correspond to $+1.0^{+1.1}_{-1.0}$ Myr for the IIAB, $+1.2^{+1.5}_{-1.4}$ Myr for the IIIAB, and $+1.6^{+1.1}_{-1.0}$ Myr for the IVA iron meteorite parent bodies. The uncertainty on these ages includes the uncertainty on the mean $\varepsilon^{182}W$ for each iron group, and the uncertainties on the CAI initial and the present-day $\varepsilon^{182}W$ of carbonaceous chondrites Eq. (1). The core formation ages for the IIAB, IIIAB and IVA iron meteorite parent bodies are indistinguishable from each other and indicate that metal segregation in these bodies occurred within less than ~1 Myr of each other. It is noteworthy that unlike the negative model ages reported in several previous studies, the core formation ages obtained here are positive. This does not only reflect the fact that the iron meteorite samples used here have only negligible cosmic ray effects, but is also due to the recent downward revision of the initial $\varepsilon^{182}W$ of CAI (Burkhardt et al., 2012).

The new Hf–W results from this study confirm earlier conclusions that accretion and core formation in the parent bodies of at least the IIAB, IIIAB, and IVA iron meteorites predated chondrule formation and the accretion of chondrite parent bodies (cf. Kleine et al., 2005a). From the new Hf–W ages and using the model for ^{26}Al heating of planetesimals from Qin et al. (2008b), we can infer accretion time scales for the IIAB, IIIAB, and IVA iron meteorite parent bodies, indicating that these bodies most likely formed within less than ~1 Myr after CAI formation and no later than ~1.5 Myr after CAI formation. In contrast, the parent bodies of chondrites appear to have formed later, as constrained by age differences between CAI and chondrules based on U–Pb and Al–Mg isotope systematics (Kita et al., 2000; Amelin et al., 2002; Kunihiro et al., 2004; Rudraswami and Goswami, 2007; Kurahashi et al., 2008). Note that chondrule formation must have predated accretion of chondrite parent bodies, so that chondrule formation ages correspond to the earliest possible accretion time for a given chondrite parent body. Available Al–Mg ages for chondrules from ordinary chondrites (L, LL) as well as CO and CR chondrites (Kita et al., 2000; Kunihiro et al., 2004; Kurahashi et al., 2008; Hutcheon et al., 2009; Kita and Ushikubo, 2012) indicate that at least these chondrite parent bodies accreted more than ~2 Myr after CAI formation, i.e., ~1 Myr later than the IIAB, IIIAB and IVA iron meteorite parent bodies. It is noteworthy that some chondrules separated from the CV chondrite Allende appear to be as old as CAI (Connolly, 2011), suggesting that some chondrite parent bodies may have accreted as early as the iron meteorite parent bodies.

5.3. Tungsten isotope anomalies and Hf–W chronometry of ungrouped iron meteorites

Apart from cosmic ray-induced shifts, the W isotopic composition of iron meteorites may vary due to the presence of nucleosynthetic isotope anomalies. Nucleosynthetic heterogeneity among bulk iron meteorite samples has been reported for several elements like Ni, Ru and Mo (Dauphas et al., 2002; Regelous et al., 2008; Chen et al., 2010; Burkhardt et al., 2011). Bulk nucleosynthetic W isotope variations have so far only been identified in CAI from Allende (Burkhardt et al., 2008, 2012) and in some members of the IVB group and ungrouped magmatic iron meteorites (Qin et al., 2008a). These anomalies could either be explained by a deficit in *s*-process or an excess in *r*-process W isotopes. Such nucleosynthetic heterogeneity could significantly affect $\varepsilon^{182}W$ and produces correlation lines in diagrams of $\varepsilon^{182}W$ vs. $\varepsilon^{183}W$, whose slopes depend on the normalisation used (Burkhardt et al., 2012) (Fig. 3).

The two ungrouped iron meteorites studied here (Chinga and Mbosi) show elevated $\varepsilon^{182}W$ (up to ~0.4 ε-units) in comparison with samples from the major groups of investigated magmatic iron meteorites (Figs. 3 and 4; Table 3). In addition, Chinga also displays elevated $\varepsilon^{183}W$ of +0.26 (Fig. 3). The higher $\varepsilon^{182}W$ in this meteorite may thus be the result of a nucleosynthetic W isotope anomaly rather than a relatively young core formation age of its parent body. The $\varepsilon^{182/184}W$ and $\varepsilon^{183/184}W$ (6/3) values of Chinga correlate as expected for *s*-process deficits (or *r*-process excesses) relative to the terrestrial composition (Fig. 3) and are consistent with nucleosynthetic effects in W isotopes observed for one other ungrouped iron meteorite (Deep Springs; Qin et al., 2008a). Correcting the measured $\varepsilon^{182/184}W$ (6/4) of Chinga using the $\varepsilon^{182}W$–$\varepsilon^{183}W$ relation for a variable distribution of *s*- and *r*-process isotopes, yields $\varepsilon^{182}W_{corr} = -3.30 \pm 0.17$, in close agreement with the measured values of the IIAB, IIIAB and IVA iron meteorite groups (Fig. 4). Thus, there appears to be no resolvable age difference between Chinga and samples from the major magmatic iron meteorite groups (Table 4).

In contrast to Chinga, Mbosi does not show evidence for nucleosynthetic isotope variation as no anomalies are observed in $\varepsilon^{183}W$. The measured $\varepsilon^{182}W$ of Mbosi, therefore, indicates that this iron meteorite is slightly younger ($\Delta t_{CAI} = +3.9 \pm 0.9$ Myr) than the other meteorites studied here. If Mbosi derived from the metallic core of a differentiated parent body, then core formation in this object occurred ~2–3 Myr later than in the IIAB, IIIAB and IVB iron meteorite parent bodies. In this case, core formation in the iron meteorite parent bodies occurred over a longer time interval than given by the Hf–W ages for the major groups of magmatic irons. Alternatively, Mbosi may have formed by a more localised metal–silicate separation event akin to those recorded in the non-magmatic iron meteorites. The metal–silicate separation age for Mbosi would in that case be consistent with ages reported for some non-magmatic iron meteorites (e.g., Kleine et al., 2005a; Schulz et al., 2012).

6. CONCLUSIONS

This study demonstrates that the cosmogenic noble gases He, Ne, and Ar are suitable for identifying iron meteorite specimens with likely minimal cosmic ray effects on W isotopes, especially if meteorites with low cosmic ray exposure ages (i.e., <60 Ma) can be identified. Based on noble gas data we selected several magmatic iron meteorite samples (including IIAB, IIIAB, IVA and IIG, as well as two ungrouped iron meteorites) that were expected to show no resolvable cosmic ray-induced effects on their W isotope compositions. With the exception of the IIG meteorite Tombigbee River all these samples have $\varepsilon^{182}W$ values identical to each other within our analytical resolution of ~0.1 ε units. All these values are slightly higher than the CAI initial, reflecting radiogenic ingrowth of ^{182}W (corresponding to ~0.1–0.2 ε-units) in a time interval between CAI formation and core formation in iron meteorite parent bodies. In contrast, samples from two meteorites with exposure ages on the order of several hundred Ma (but still with low concentrations of cosmogenic noble gases) show $\varepsilon^{182}W$ values scattering towards more negative values, some of which are lower than the CAI initial. This demonstrates that cosmic ray-induced neutron capture reactions on W isotopes even affected iron meteorite samples having low concentrations of cosmogenic noble gases, if these samples stem from relatively well shielded positions in large meteoroids with long exposure times.

The W isotopic compositions of iron meteorites with negligible cosmic ray effects indicate that core formation in the IIAB, IIIAB and IVA iron meteorite parent bodies occurred $+1.0^{+1.1}_{-1.0}$ Myr, $+1.2^{+1.5}_{-1.4}$ Myr, and $+1.6^{+1.1}_{-1.0}$ Myr after CAI formation, respectively, and that metal segregation in these bodies occurred within a brief time interval of less than ~1 Myr of each other. In contrast, one ungrouped iron meteorite (Mbosi) derives from a parent body that underwent metal–silicate separation 2–3 Myr later than the major magmatic iron meteorite groups. The new Hf–W results are consistent with conclusions of earlier studies that accretion and core formation of the parent bodies of magmatic iron meteorites predated accretion of chondrite parent bodies. However, unlike the sometimes negative model ages obtained in some previous Hf–W studies on magmatic iron meteorites, the ages obtained here are all positive and consistent with the results of a previous study that used physical models to correct for cosmic ray effects on W isotope compositions of iron meteorites. The major advance of the present study, however, is the identification of samples that remained essentially unaffected by cosmic rays, and thus require no correction on their measured $\varepsilon^{182}W$ at all.

While this study demonstrates that iron meteorites with low cosmic ray exposure ages are well suited to determine W isotopic compositions essentially unmodified by cosmic ray interactions, such samples are rare. Furthermore, Tombigbee River likely shows neutron capture effects on its W isotope composition in spite of very low concentrations of cosmogenic noble gases. In such cases, even a short second stage exposure derived from a low noble gas concentration (perhaps in conjunction with a cosmogenic radionuclide

analysis) may not guarantee a negligible (epi)thermal neutron fluence during a first irradiation at larger shielding. The comprehensive application of Hf–W chronometry to all known groups of iron meteorites, therefore, requires the development of a direct neutron dosimeter that will permit the full quantification of neutron capture-induced W isotope shifts in iron meteorites with longer exposure ages (>100 Ma). Initial results suggest that Pt isotopes may be a suitable neutron dosimeter for iron meteorites and an appropriate proxy for neutron capture-induced shifts in W isotopes. Nevertheless, future studies employing such a direct neutron dosimeter will profit from analysis of the weakly irradiated samples identified in this study. As such samples essentially require no correction, they will be key samples to firmly establish the Hf–W chronology of iron meteorites.

ACKNOWLEDGEMENTS

F. Brandstätter (Naturhistorisches Museum Wien), D. Ebel and J. Boesenberg (American Museum of Natural History, New York), B. Hofmann (Naturhistorisches Museum Bern), M. Honda (Tokyo), A. Locock and C. Herd (Univ. Alberta, Edmonton), K. Marti (Univ. California, San Diego), J. Nauber (JNMC, Zürich), and J. Zipfel (Forschungsinstitut und Naturmuseum Senckenberg, Frankfurt) are gratefully acknowledged for providing samples. Thomas Kruijer thanks F. Oberli, L. Huber, N. Dalcher and M. Cosarinsky for advice. The very detailed and constructive comments by Larry Nyquist are gratefully acknowledged. This paper greatly benefited from constructive reviews by Nicolas Dauphas and Larry Nyquist and the editorial efforts of Greg Herzog. This study was supported by the Schweizerische Nationalfonds (SNF Grant PP00P2_123470 to T. Kleine).

REFERENCES

Amelin Y., Kaltenbach A., Iizuka T., Stirling C. H., Ireland T. R., Petaev M. and Jacobsen S. B. (2010) U–Pb chronology of the solar system's oldest solids with variable (238)U/(235)U. *Earth Planet. Sci. Lett.* **300**, 343–350.

Amelin Y., Krot A. N., Hutcheon I. D. and Ulyanov A. A. (2002) Lead isotopic ages of chondrules and calcium-aluminum-rich inclusions. *Science* **297**, 1678–1683.

Ammon K., Leya I. and Lin Y. (2011) Noble gases in the Xinjiang (Armanty) iron meteorite – a big object with a short cosmic-ray exposure age. *Meteorit. Planet. Sci.* **46**, 785–792.

Ammon K., Masarik J. and Leya I. (2008) Noble gases in Grant and Carbo and the influence of S- and P-rich mineral inclusions on the K-41-K-40 dating system. *Meteorit. Planet. Sci.* **43**, 685–699.

Ammon K., Masarik J. and Leya I. (2009) New model calculations for the production rates of cosmogenic nuclides in iron meteorites. *Meteorit. Planet. Sci.* **44**, 485–503.

Arlandini C., Kappeler F., Wisshak K., Gallino R., Lugaro M., Busso M. and Straniero O. (1999) Neutron capture in low-mass asymptotic giant branch stars: cross sections and abundance signatures. *Astrophys. J.* **525**, 886–900.

Bouvier A. and Wadhwa M. (2010) The age of the solar system redefined by the oldest Pb–Pb age of a meteoritic inclusion. *Nat. Geosci.* **3**, 637–641.

Burkhardt C., Kleine T., Bourdon B., Palme H., Zipfel J., Friedrich J. M. and Ebel D. S. (2008) Hf–W mineral isochron for Ca, Al-rich inclusions: age of the solar system and the timing of core formation in planetesimals. *Geochim. Cosmochim. Acta* **72**, 6177–6197.

Burkhardt C., Kleine T., Dauphas N. and Wieler R. (2012) Nucleosynthetic tungsten isotope anomalies in acid leachates of the Murchison chondrite: implications for hafnium–tungsten chronometry. *Astrophys. J. Lett.* **753**, L6.

Burkhardt C., Kleine T., Oberli F., Pack A., Bourdon B. and Wieler R. (2011) Molybdenum isotope anomalies in meteorites: constraints on solar nebula evolution and origin of the Earth. *Earth Planet. Sci. Lett.* **312**, 390–400.

Chang C. and Wänke H. (1969) Beryllium-10 in iron meteorites, their cosmic-ray exposure and terrestrial ages. In *Meteorite Research* (ed. P. Millman). Reidel, Dordrecht, The Netherlands.

Chen J. H., Papanastassiou D. A. and Wasserburg G. J. (2010) Ruthenium endemic isotope effects in chondrites and differentiated meteorites. *Geochim. Cosmochim. Acta* **74**, 3851–3862.

Chen J. H. and Wasserburg G. J. (1990) The isotopic composition of Ag in meteorites and the presence of Pd-107 in protoplanets. *Geochim. Cosmochim. Acta* **54**, 1729–1743.

Cobb J. C. (1966) Iron meteorites with low cosmic ray exposure ages. *Science* **151**, 1524.

Connolly H. C. et al. (2011) Diffusion within the CAI Bocce Ball 1: the distribution of $^{26}Mg^{*}$ correlated with variations in Al/Mg within a type B2 inclusion from Allende. *42nd Lunar and Planetary Science Conference*, Houston, Texas. #1858.

Dauphas N., Marty B. and Reisberg L. (2002) Molybdenum evidence for inherited planetary scale isotope heterogeneity of the protosolar nebula. *Astrophys. J.* **565**, 640–644.

Eugster O. (2003) Cosmic-ray exposure ages of meteorites and lunar rocks and their significance. *Chem. Erde: Geochem.* **63**, 3–30.

Gray C. M., Papanastassiou D. A. and Wasserburg G. J. (1973) Identification of early condensates from the solar nebula. *Icarus* **20**, 213–239.

Harper C. L. and Jacobsen S. B. (1996) Evidence for Hf-182 in the early solar system and constraints on the timescale of terrestrial accretion and core formation. *Geochim. Cosmochim. Acta* **60**, 1131–1153.

Honda A., Nagai H., Nagao K., Bajo K., Takaoka N., Oura Y. and Nishiizumi K. (2009) Irradiation histories of iron meteorites. *Proc. Int. Workshop Adv. Cosmic Ray Sci.* **78**, 12–17.

Horan M. F., Smoliar M. I. and Walker R. J. (1998) ^{182}W and ^{187}Re–^{187}Os systematics of iron meteorites: chronology for melting, differentiation, and crystallization in asteroids. *Geochim. Cosmochim. Acta* **62**, 545–554.

Hutcheon I. D., Marhas K. K., Krot A. N., Goswami J. N. and Jones R. H. (2009) ^{26}Al in plagioclase-rich chondrules in carbonaceous chondrites: evidence for an extended duration of chondrule formation. *Geochim. Cosmochim. Acta* **73**, 5080–5099.

Kita N. T., Nagahara H., Togashi S. and Morishita Y. (2000) A short duration of chondrule formation in the solar nebula: evidence from ^{26}Al in Semarkona ferromagnesian chondrules. *Geochim. Cosmochim. Acta* **64**, 3913–3922.

Kita N. T. and Ushikubo T. (2012) Evolution of protoplanetary disk inferred from ^{26}Al chronology of individual chondrules. *Meteorit. Planet. Sci.* **47**, 1108–1119.

Kleine T., Mezger K., Munker C., Palme H. and Bischoff A. (2004) Hf-182–W-182 isotope systematics of chondrites, eucrites, and martian meteorites: chronology of core formation and early mantle differentiation in Vesta and Mars. *Geochim. Cosmochim. Acta* **68**, 2935–2946.

Kleine T., Mezger K., Palme H., Scherer E. and Munker C. (2005a) Early core formation in asteroids and late accretion of chondrite parent bodies: evidence from Hf-182–W-182 in CAIs,

metal-rich chondrites, and iron meteorites. *Geochim. Cosmochim. Acta* **69**, 5805–5818.

Kleine T., Munker C., Mezger K. and Palme H. (2002) Rapid accretion and early core formation on asteroids and the terrestrial planets from Hf–W chronometry. *Nature* **418**, 952–955.

Kleine T., Palme H., Mezger M. and Halliday A. N. (2005b) Hf–W chronometry of lunar metals and the age and early differentiation of the Moon. *Science* **310**, 1671–1674.

Kleine T., Touboul M., Bourdon B., Nimmo F., Mezger K., Palme H., Jacobsen S. B., Yin Q. Z. and Halliday A. N. (2009) Hf–W chronology of the accretion and early evolution of asteroids and terrestrial planets. *Geochim. Cosmochim. Acta* **73**, 5150–5188.

Kleine T., Touboul M., Van Orman J. A., Bourdon B., Maden C., Mezger K. and Halliday A. N. (2008) Hf–W thermochronometry: closure temperature and constraints on the accretion and cooling history of the H chondrite parent body. *Earth Planet. Sci. Lett.* **270**, 106–118.

Kollár D., Michel R. and Masarik J. (2006) Monte Carlo simulation of GCR neutron capture production of cosmogenic nuclides in stony meteorites and lunar surface. *Meteorit. Planet. Sci.* **41**, 375–389.

Kruijer T. S., Fischer-Gödde M., Sprung P., Leya I., Wieler R. and Kleine T. (2012) Neutron capture on platinum and tungsten isotopes in iron meteorites: implications for Hf–W chronometry. *43rd Lunar and Planetary Science Conference*, Houston, Texas. #1529.

Kunihiro T., Rubin A. E., McKeegan K. D. and Wasson J. T. (2004) Initial Al-26/Al-27 in carbonaceous-chondrite chondrules: too little Al-26 to melt asteroids. *Geochim. Cosmochim. Acta* **68**, 2947–2957.

Kurahashi E., Kita N. T., Nagahara H. and Morishita Y. (2008) ^{26}Al–^{26}Mg systematics of chondrules in a primitive CO chondrite. *Geochim. Cosmochim. Acta* **72**, 3865–3882.

Lee D. C. and Halliday A. N. (1995) Hafnium–tungsten chronometry and the timing of terrestrial core formation. *Nature* **378**, 771–774.

Lee D. C., Halliday A. N., Leya I., Wieler R. and Wiechert U. (2002) Cosmogenic tungsten and the origin and earliest differentiation of the moon. *Earth Planet. Sci. Lett.* **198**, 167–175.

Leya I. and Masarik J. (2009) Cosmogenic nuclides in stony meteorites revisited. *Meteorit. Planet. Sci.* **44**, 1061–1086.

Leya I., Wieler R. and Halliday A. N. (2000) Cosmic-ray production of tungsten isotopes in lunar samples and meteorites and its implications for Hf–W cosmochemistry. *Earth Planet. Sci. Lett.* **175**, 1–12.

Leya I., Wieler R. and Halliday A. N. (2003) The influence of cosmic-ray production on extinct nuclide systems. *Geochim. Cosmochim. Acta* **67**, 529–541.

Lingenfelter R. E., Canfield E. H. and Hampel V. E. (1972) The lunar neutron-flux revisited. *Earth Planet. Sci. Lett.* **16**, 355–369.

Markowski A., Leya I., Quitté G., Ammon K., Halliday A. N. and Wieler R. (2006a) Correlated helium-3 and tungsten isotopes in iron meteorites: quantitative cosmogenic corrections and planetesimal formation times. *Earth Planet. Sci. Lett.* **250**, 104–115.

Markowski A., Quitté G., Halliday A. N. and Kleine T. (2006b) Tungsten isotopic compositions of iron meteorites: chronological constraints vs. cosmogenic effects. *Earth Planet. Sci. Lett.* **242**, 1–15.

Masarik J. (1997) Contribution of neutron capture reactions to observed tungsten isotopic ratios. *Earth Planet. Sci. Lett.* **152**, 181–185.

Mathew K. J. and Marti K. (2009) Galactic cosmic ray-produced (129)Xe and (131)Xe excesses in troilites of the Cape York iron meteorite. *Meteorit. Planet. Sci.* **44**, 107–114.

Qin L. P., Dauphas N., Wadhwa M., Markowski A., Gallino R., Janney P. E. and Bouman C. (2008a) Tungsten nuclear anomalies in planetesimal cores. *Astrophys. J.* **674**, 1234–1241.

Qin L. P., Dauphas N., Wadhwa M., Masarik J. and Janney P. E. (2008b) Rapid accretion and differentiation of iron meteorite parent bodies inferred from Hf-182–W-182 chronometry and thermal modeling. *Earth Planet. Sci. Lett.* **273**, 94–104.

Regelous M., Elliott T. and Coath C. D. (2008) Nickel isotope heterogeneity in the early solar system. *Earth Planet. Sci. Lett.* **272**, 330–338.

Rudraswami N. G. and Goswami J. N. (2007) Al-26 in chondrules from unequilibrated L chondrites: onset and duration of chondrule formation in the early solar system. *Earth Planet. Sci. Lett.* **257**, 231–244.

Scherstén A., Elliott T., Hawkesworth C., Russell S. and Masarik J. (2006) Hf–W evidence for rapid differentiation of iron meteorite parent bodies. *Earth Planet. Sci. Lett.* **241**, 530–542.

Schönberg R., Kamber B. S., Collerson K. D. and Eugster O. (2002) New W-isotope evidence for rapid terrestrial accretion and very early core formation. *Geochim. Cosmochim. Acta* **66**, 3151–3160.

Schultz L. and Franke L. (2004) *Helium, Neon & Argon in Meteorites: A Data Collection*. Max-Planck-Institut für Geochemie, Mainz (Germany).

Schulz T., Upadhyay D., Münker C. and Mezger K. (2012) Formation and exposure history of non-magmatic iron meteorites and winonaites: clues from Sm and W isotopes. *Geochim. Cosmochim. Acta* **85**, 200–212.

Scott E. R. D. (1972) Chemical fractionation in iron-meteorites and its interpretation. *Geochim. Cosmochim. Acta* **36**, 1205–1236.

Scott E. R. D. and Wasson J. T. (1975) Classification and properties of iron-meteorites. *Rev. Geophys.* **13**, 527–546.

Signer P. and Nier A. O. (1960) The distribution of cosmic-ray-produced rare gases in iron meteorites. *J. Geophys. Res.* **65**, 2947–2964.

Smoliar M. I., Walker R. J. and Morgan J. W. (1996) Re–Os ages of group IIA, IIIA, IVA, and IVB iron meteorites. *Science* **271**, 1099–1102.

Sprung P., Scherer E. E., Upadhyay D., Leya I. and Mezger K. (2010) Non-nucleosynthetic heterogeneity in non-radiogenic stable Hf isotopes: implications for early solar system chronology. *Earth Planet. Sci. Lett.* **295**, 1–11.

Vockenhuber C., Oberli F., Bichler M., Ahmad I., Quitte G., Meier M., Halliday A. N., Lee D. C., Kutschera W., Steier P., Gehrke R. J. and Helmer R. G. (2004) New half-life measurement of Hf-182: improved chronometer for the early solar system. *Phys. Rev. Lett.* **93**.

Voshage H. (1978) Investigations on cosmic-ray-produced nuclides in iron-meteorites: 2. New results on K-41–K-40–He-4–Ne-21 exposure ages and interpretation of age distributions. *Earth Planet. Sci. Lett.* **40**, 83–90.

Voshage H. (1984) Investigations of cosmic-ray-produced nuclides in iron-meteorites: 6. The Signer–Nier model and the history of the cosmic-radiation. *Earth Planet. Sci. Lett.* **71**, 181–194.

Walker R. J. and Touboul M. (2012) Improved constraints on the relative timing of metal segregation in the early solar system using coupled W–Os isotopes. *43rd Lunar and Planetary Science Conference*, Houston, Texas. #1166.

Welten K. C., Nishiizumi K., Lavielle B., Caffee M. W., Hillegonds D. J., Finkel R. C., Kollar D. and Masarik J. (2008) The complex exposure histories of the Pitts and Horse Creek iron meteorites: implications for meteorite delivery models. *Meteorit. Planet. Sci.* **43**, 1321–1332.

Wieler R. (2002) Cosmic-ray-produced noble gases in meteorites. *Noble Gases Geochem. Cosmochem.* **47**, 125–170.

Wieler R., Beer J. and Leya I. (2011) The galactic cosmic ray intensity over the past 106–109 years as recorded by cosmogenic nuclides in meteorites and terrestrial samples. *Space Sci. Rev.*. http://dx.doi.org/10.1007/s11214-11011-19769-11219.

Willbold M., Elliott T. and Moorbath S. (2011) The tungsten isotopic composition of the Earth's mantle before the terminal bombardment. *Nature* **477**, 195-U91.

Wittig N., Humayun M., Huang S. and Brandon A. D. (2012) Revised tungsten isotope chronology of IVB iron meteorites from W–Os systematics. *43rd Lunar and Planetary Science Conference*, Houston, Texas. #1482.

Yin Q. Z., Jacobsen S. B., Yamashita K., Blichert-Toft J., Telouk P. and Albarede F. (2002) A short timescale for terrestrial planet formation from Hf–W chronometry of meteorites. *Nature* **418**, 949–952.

Associate editor: Gregory F. Herzog